

EMPIRICAL AND BIOPHYSICAL MODELING STUDIES OF DISPERSAL BARRIERS  
FOR MARINE PLANKTON

A THESIS SUBMITTED TO THE GRADUATE DIVISION OF THE UNIVERSITY OF  
HAWAI'I AT MĀNOA IN PARTIAL FULFILLMENT OF THE REQUIREMENTS FOR THE  
DEGREE OF

MASTER OF SCIENCE

IN

OCEANOGRAPHY

AUGUST 2013

By

Emily L. Norton

Thesis Committee:

Erica Goetze, Chairperson

Anna Neuheimer

Brian Powell

Robert Toonen

Keywords: connectivity, copepod, genetic structure, holoplankton, mtCOII, SODA

©Copyright 2013, Emily L. Norton

## **Acknowledgments**

I would like to thank my advisor, Erica Goetze, for her thoughtful guidance and active support throughout my master's project. I would also like to thank Brian Powell for inspiring me to become a modeler; Anna Neuheimer for coding beside me and teaching me that the computer is always right; and Rob Toonen for helping me understand the power and limitations of molecular work. Thank you all for the advice and feedback you have given to improve this project from the nascent to final stages.

Chapter 1: We thank R. Harmer, V. Flynn, L. Johnson, and E. Portner for field and laboratory assistance, and K. Andrews and R. Toonen for insights on data analysis. We also thank two anonymous reviewers for thoughtful comments on the manuscript. This work was supported by the National Science Foundation, under Ocean Sciences grant 1029478, and a Waitt Foundation – National Geographic grant (W119-10) to E. Goetze. The Atlantic Meridional Transect (AMT) sampling also was supported by the UK Natural Environment Research Council National Capability funding to Plymouth Marine Laboratory and the National Oceanography Centre, Southampton. This is contribution number 227 of the AMT programme. This chapter is in press in *Limnology and Oceanography*, and the authorship is Norton & Goetze.

Chapter 2: We thank K. Andrews for suggestions on the manuscript. This work was supported by NSF grant OCE-1029478 to E. Goetze. This chapter has not yet been submitted for publication, and expected authorship is Norton, Powell, Neuheimer, and Goetze.

## Abstract

Because there are few obvious dispersal barriers in the open ocean, pelagic organisms are typically expected to experience high connectivity over long distances. However, very little work has been done to understand gene flow in pelagic holoplankton on a global scale. In this study, I investigated genetic connectivity among populations of the mesopelagic copepod, *Haloptilus longicornis*, using both empirical and biophysical modeling approaches. Using the mitochondrial marker, cytochrome oxidase subunit II (mtCOII, 43 locations, N = 1059), highly significant genetic structure was detected among ocean basins (global  $F_{ST} = 0.20$ ;  $p < 0.00001$ ), with the exception of a lack of genetic structure between South Atlantic and Indian Ocean populations of *H. longicornis*. Genetic breaks were also detected among subtropical gyre populations within the Atlantic and Pacific Oceans in this species (Atlantic:  $F_{CT} = 0.21$ , Pacific:  $F_{CT} = 0.15$ , AMOVA,  $p < 0.00001$  for both oceans). I tested for Isolation by Distance (IBD) on the basin and gyre scales in the Atlantic and Pacific, and observed a significant relationship between genetic and geographic distance for basin-wide comparisons ( $p < 0.01$  for Mantel; linear regression:  $R^2 = 0.142$  for Pacific,  $R^2 = 0.266$  for Atlantic;  $p < 0.001$  for both); however, there was no pattern of IBD for the within-gyre comparisons in any of the four subtropical gyres ( $p \gg 0.05$  for all). In combination, these results suggest that the significant result for IBD in the basin-scale comparisons was driven by the equatorial genetic breaks observed in both the Atlantic and Pacific Oceans. In the Atlantic Ocean, the equatorial genetic break was accompanied by low abundance of *H. longicornis* (0-12°N), and pilot studies indicated that reproductive failure was high in this region. These results indicate that the equatorial region may be poor quality habitat for this species and serve as a biophysical dispersal barrier to migrants traveling among subtropical gyre habitats. In order to better understand contemporary dispersal patterns and the

mechanism underlying this dispersal barrier in the Atlantic Ocean, I simulated particle dispersal for 30 years using the Simple Ocean Data Assimilation (SODA) model coupled with a particle-tracking scheme. Particle dispersal was simulated using physical forcing alone and in combination with increased mortality or decreased reproduction in the equatorial region, in order to determine whether a physical or a biophysical dispersal barrier exists in the equatorial Atlantic. Particle dispersal forced with physical oceanographic processes predicted that 26% of particles originating in the southern gyre dispersed to the northern gyre over the 30-year simulation, which is an unrealistically high rate of connectivity given the empirical genetic divergence observed among these populations. When conservative biological processes were imposed in the equatorial region, connectivity among populations in the northern and southern subtropical gyres ceased. These results suggest that the dispersal barrier across the equatorial region must be biophysical in nature, and that it likely prevents contemporary dispersal among subtropical gyre populations. Therefore, populations of *H. longicornis* in the subtropical gyres of the northern and southern Atlantic are demographically as well as genetically isolated, and may evolve independently in response to local selective pressures. This is the first study on marine holoplankton to compare biophysical modeling predictions with empirical genetic data in order to identify the mechanism underlying a pelagic dispersal barrier.

## Table of Contents

Acknowledgments.....	iii
Abstract.....	iv
List of Tables .....	vii
List of Figures.....	viii
Chapter 1: Equatorial dispersal barriers and limited population connectivity among oceans in a planktonic copepod.....	1
Abstract.....	1
Introduction.....	3
Methods.....	6
Results.....	13
Discussion.....	19
References Cited.....	26
Tables.....	33
Figures.....	36
Chapter 2: A biophysical dispersal barrier for holoplankton in the equatorial Atlantic.....	45
Abstract.....	45
Introduction.....	46
Methods.....	51
Results.....	59
Discussion.....	64
References Cited.....	71
Tables.....	81
Figures.....	83
Future work.....	95

## List of Tables

### Chapter 1:

<b>Table 1</b> .....	33
Population samples and summary statistics for the <i>Haloptilus longicornis</i> genetic study.	
<b>Table 2</b> .....	34
$D_{est}$ and pairwise $F_{ST}$ values between all collection sites.	
<b>Table 3</b> .....	35
Analysis of molecular variance (AMOVA) results comparing northern and southern gyre populations of <i>H. longicornis</i> in the Atlantic and Pacific Oceans.	

### Chapter 2:

<b>Table 1</b> .....	81
Station locations for genetic data and particle releases for the Isolation by Oceanographic Distance (IBOD) portion of the modeling study.	
<b>Table 2</b> .....	82
Pairwise $F_{ST}$ values between all collection sites in the Atlantic Ocean.	

## List of Figures

### Chapter 1:

<b>Figure 1</b> .....	36
Global map of collection sites for populations included in the genetic study.	
<b>Figure 2</b> .....	37
Statistical parsimony haplotype network for mtCOII haplotypes in <i>H. longicornis</i> .	
<b>Figure 3</b> .....	38
Map of mtCOII haplotype frequencies sampled at each collection site in the Indian and Pacific Oceans.	
<b>Figure 4</b> .....	39
Environmental portrait of an open-ocean dispersal barrier for <i>H. longicornis</i> in the Atlantic Ocean.	
<b>Figure 5</b> .....	41
Results of principal coordinates analysis (PCoA) of all samples, based on pairwise $F_{ST}$ values.	
<b>Figure 6</b> .....	42
Genetic distance (Linearized $F_{ST}$ ) regressed against geographic distance to test for isolation by distance within four subtropical gyres (Pacific, Atlantic).	
<b>Figure 7</b> .....	43
Genetic distance (Linearized $F_{ST}$ ) regressed against geographic distance to test for isolation by distance at basin scales in the Atlantic and Pacific Oceans.	
<b>Figure S1</b> .....	44

Population graph for all collection sites.

**Chapter 2:**

**Figure 1** .....83

Average current velocities at 197 m depth for the ocean circulation model, SODA.

**Figure 2** .....84

Map of the Atlantic Ocean divided into 15 Longhurst provinces.

**Figure 3** .....85

Theoretical curves showing the decline in population size over time when increased mortality or decreased reproduction were imposed in the equatorial region.

**Figure 4** .....86

Station locations in the Atlantic Ocean at which particles were released in the Isolation by Oceanographic Distance (IBOD) simulations.

**Figure 5** .....87

Connectivity matrices showing the change in dispersal patterns among 15 regions in the Atlantic Ocean between year 1 and year 30 of the simulations.

**Figure 6** .....89

Migration among Atlantic subtropical gyres, over a 30-year simulation.

**Figure 7** .....90

Residence times in the Atlantic equatorial region for particles dispersing among subtropical gyres.

**Figure 8** .....91

Dispersal trajectories for the fastest particles traveling from the southern to the northern subtropical gyre.

**Figure 9** .....92

Death locations in the equatorial region for particles dispersing among subtropical gyres when increased mortality and decreased reproduction were imposed.

**Figure 10** .....93

Connectivity among Atlantic Stations when particles were advected with physical forcing alone and when mortality was imposed in the equatorial region.

**Figure 11** .....94

Genetic distance (Linearized  $F_{ST}$ ) versus dispersal probability for within-gyre comparisons, when mortality was simulated in the equatorial region.

## **Chapter 1:** Equatorial dispersal barriers and limited population connectivity among oceans in a planktonic copepod

### **Abstract**

Because there are few obvious dispersal barriers in the open ocean, pelagic organisms are typically expected to experience gene flow over long distances. However, very little empirical work has been done to understand gene flow in pelagic holoplankton on a global scale. In this study, we investigated population genetic structure within and between ocean basins in the common mesopelagic copepod, *Haloptilus longicornis*, using the mitochondrial marker cytochrome oxidase subunit II (mtCOII, 43 locations,  $n = 1059$ ). We found highly significant genetic structure among ocean basins (global  $F_{ST} = 0.20$ ;  $p < 0.00001$ ), with the exception of relatively weak genetic divergence between the South Atlantic and Indian Oceans. Strong genetic breaks also were observed between populations in the northern and southern subtropical gyres of both the Atlantic and Pacific Oceans (Atlantic:  $F_{CT} = 0.21$ , Pacific:  $F_{CT} = 0.15$ , AMOVA,  $p < 0.00001$  for both oceans). In the Atlantic, a region of low abundance for *H. longicornis* in equatorial waters coincided with the location of the observed genetic break ( $\sim 0$ - $12^\circ$  N), suggesting the presence of a physical or biophysical barrier that effectively limits migration among subtropical gyre systems for this species. Using oceanographic data from a basin-scale transect, we provide the first environmental portrait of an open-ocean dispersal barrier for the marine plankton. Within all four Atlantic and Pacific subtropical gyres, we found a general lack of genetic subdivision among sites, as has been observed in a few other globally-distributed plankton species.



## Introduction

Relatively little is known about the genetic structure of holozooplankton, despite their high abundance in the ocean and their ecological importance at intermediate trophic levels in pelagic marine food webs. Due to the lack of obvious physical barriers in the open ocean, it has been hypothesized that zooplankton experience nearly unlimited dispersal among widespread populations (Norris 2000). In addition, the large effective population sizes of zooplankton species should minimize genetic drift (Bucklin and Wiebe 1998; Peijnenburg et al. 2005). Therefore, it is often predicted that marine plankton will exhibit low population genetic structure even between geographically distant populations (Peijnenburg et al. 2005; Provan et al. 2009). However, many empirical studies have detected genetic structure over a range of spatial scales, including between ocean basins, between gyres within an ocean basin, and regionally among coastal embayments and estuaries (Papetti et al. 2005; Blanco-Bercial et al. 2011; Chen and Hare 2011). Additionally, genetic structure sometimes differs between holoplanktonic species collected at the same sites (e.g., *Calanus* spp. vs. *Acartia clausi*, Bucklin et al. 2000; Goetze 2005, 2011). These results indicate that population genetic structure may be prevalent and complex in marine zooplankton, contrary to prior predictions.

It is currently unknown for holozooplankton what characteristics of an organisms' life history, behavior, and habitat are important drivers of dispersal and connectivity among populations, because few species have been studied and these studies usually only sampled over a portion of the distributional range. A far more extensive literature exists for nearshore, meroplanktonic species (reviewed by Cowen and Sponaugle 2009), and these studies suggest that both biological and physical factors affect connectivity. Biological characteristics, such as swimming ability, homing behaviors, diel vertical migration (DVM) behavior, and habitat depth

preference have been shown to influence dispersal in meroplanktonic species with a benthic or demersal adult stage, as well as in large pelagic vertebrate predators (Cronin and Forward 1986; Alvarado Bremer et al. 2005; Gerlach et al. 2007). Additionally, modeling studies have shown that physical factors, such as oceanographic current velocity and seasonal changes in current structure, which control transport time between sites, can affect dispersal in meroplankton (Baums et al. 2006; White et al. 2010). Habitat continuity also influences genetic structure in a variety of shallow-water, demersal or benthic organisms (Johnson and Black 1995; Alberto et al. 2010). Since holoplankton do not require neritic habitats, we expect that different ocean features will serve as dispersal barriers for these species, but limited dispersal due to biological or physical factors also may be important in determining population connectivity within holoplankton.

In this study, we investigated global and basin-scale patterns of population genetic structure in the marine holoplanktonic copepod *Haloptilus longicornis*. This species occurs in tropical and subtropical waters of every ocean basin (Fig. 1), and can tolerate a wide range of environmental conditions (Saraladevi et al. 1979; Razouls et al. 2005-2012). *Haloptilus longicornis* has a primary depth habitat of ~100-400 m, does not exhibit diel vertical migration behavior, and is the most abundant upper mesopelagic plankton species in many ocean ecosystems (McGowan and Walker 1979; Saraladevi et al. 1979; Ambler and Miller 1987). This species is likely globally important in pelagic ecosystems due to its cosmopolitan distribution and high abundance, but it has been little studied. To our knowledge, no information is available on the life history, reproduction, or diet of *H. longicornis* or any of its close relatives. However, it is known that the preferred habitat depth of *H. longicornis* is characteristic for a number of

other mesozooplankton species (McGowan and Walker 1979), making this a model taxon for understanding how habitat depth may influence genetic structure in planktonic species.

Using mitochondrial cytochrome oxidase subunit II (mtCOII) sequences from 1059 specimens, and abundance data for *H. longicornis* from 33 collection sites in the Atlantic Ocean, we describe global patterns of genetic structure and identify suitable habitat for this species in the Atlantic to address the following central questions: 1) Are there genetic breaks between ocean basins or between subtropical gyre systems within ocean basins? 2) Do *H. longicornis* populations show a pattern of isolation by distance (IBD) at basin or ocean gyre scales in the Atlantic and Pacific Oceans? 3) Using *H. longicornis* abundance measurements and environmental data for the Atlantic, can we identify areas of suitable habitat for this species and describe potential oceanic barriers to dispersal? Due to the cosmopolitan distribution and upper mesopelagic depth habitat of *H. longicornis*, we expected that continental land masses and the shallow Sunda shelf in the Indo-Pacific region would serve as dispersal barriers between ocean basins. Therefore, we predicted high genetic divergence between populations in the Atlantic, Indian, and Pacific Oceans. Because of the upper mesopelagic depth habitat and lack of DVM in this species, we expected that animals would be entrained in the upper ocean circulation. Since near-surface currents circulate primarily on the sub-basin scale, we predicted strong genetic structure between subtropical gyres within the Atlantic and Pacific Oceans. Here we show that range-wide population genetic structure is strong in this species, and that equatorial waters serve as a barrier to dispersal between northern and southern subtropical gyres in both the Atlantic and Pacific Oceans.

## Methods

### *Specimen collection*

*Haloptilus longicornis* was collected from 43 sites in the Atlantic, Pacific, and Indian Oceans as well as the Mediterranean Sea (Table 1; Fig. 1). The Mediterranean Sea is the type locality for this species (Claus 1863). In the Indian, Pacific, and North Atlantic (MP3 cruise; Table 1), bulk plankton was collected by oblique tows of either a 0.71 m diameter bongo net or a 1 m diameter ring net with mesh sizes 202 – 333  $\mu\text{m}$ , between 200 – 1000 m and the surface. These samples were non-quantitative. On the 2010 Atlantic Meridional Transect cruise (AMT20), bulk plankton was collected on a transect between the United Kingdom and southern Chile using a 0.57 m diameter bongo net (total area = 0.25 m<sup>2</sup>), towed vertically between 200 – 300 m and the surface. On this cruise, deeper tows (300 – 0 m) were conducted at 22 sites between 49° N and 6° S (Sites 25-26, 30-33, 36-37), and shallower tows (200 – 0 m) were conducted between 12° S and 44° S (Sites 22-24). The 2010 AMT bongo samples were quantitative. Upon recovery of the net, bulk plankton was preserved immediately in 95 – 100% non-denatured ethyl alcohol, changed to new alcohol within 12-24 hours after collection, and stored at -20°C. Adult female *H. longicornis* were sorted from preserved bulk plankton samples in the laboratory. *Haloptilus longicornis* specimens were distinguished from closely related species by head shape, presence of a distinctive median papilla, body size, genital segment shape, and antennule length (Sars 1902; Mori 1964; Bradford-Grieve 1999). Only adult females were used because males and copepodites are more difficult to identify to species, and they were rare in most of our samples.

*Deoxyribonucleic acid (DNA) extraction, Polymerase chain reaction (PCR), and sequencing*

DNA was extracted from individual adult *H. longicornis* using the Qiagen DNeasy Blood and Tissue Kit. The manufacturer's extraction protocol was modified in order to maximize the amount of DNA recovered from these small-bodied copepods by: 1) pulverizing the entire copepod to increase cell lysis, 2) halving most reagent volumes, 3) extending the final room-temperature incubation to 10 minutes, and 4) eluting DNA twice instead of once.

Initial DNA sequence for mtCOII was obtained using universal primers COII\_F2 (5' – GGT CAA TTT GGT CTA CAG GAT GC – 3') and COII\_R4 (5' – TGA TTA GCC CCA CAA ATC TCA G – 3'), which were developed from *Pareucalanus attenuatus* and *Euchaeta rimana* mtCOII sequence data (K. Halbert and E. Goetze unpubl.) Using these data we designed new, species-specific primers for mtCOII that resulted in clean and reliable amplification of a 546 base pair (bp) fragment of this gene (COII\_F6: 5' – GTC TAC AGG ATG CAA ACT CC – 3' and COII\_R9: 5' – AGA GCA TTG CCC AAA CCT GA – 3'). PCR amplifications were conducted in 25  $\mu\text{L}$  volumes with 2.25  $\mu\text{L}$  of 10X buffer, 0.2  $\text{mmol L}^{-1}$  deoxyribonucleotide triphosphates (dNTPs), 1.5  $\text{mmol L}^{-1}$   $\text{MgCl}_2$ , 0.3  $\mu\text{mol L}^{-1}$  of each primer, 0.08  $\text{U } \mu\text{L}^{-1}$  Taq polymerase (Bioline), and 3  $\mu\text{L}$  of template DNA. The PCR protocol was 2 minutes at 95°C, followed by 40 cycles of 30 seconds at 95°C, 30 seconds at 53°C, and 1 minute at 72°C, and completed with 4 minutes at 72°C. PCR products were run on a 1.5-2% agarose gel for visualization. PCR products were purified using Exonuclease I (0.5 units; USB Corporation) and Shrimp Alkaline Phosphatase (0.25 units; USB Corporation) for 30 minutes at 37°C, followed by 15 minutes at 95°C. Sanger sequencing was used to obtain both forward and reverse sequences of mtCOII from 1059 specimens (Table 1). Thirty-four of these specimens were collected in the tropical Atlantic (AMT20 – 17 to 20; 2.0 – 10.6°N; Fig. 1). Sequences from these 34 individuals

were included in statistical parsimony network analyses, but were omitted from population-level analyses due to low sample sizes ( $n = 5 - 15$  individuals per sample).

Initially, we had planned to use a fragment of the mitochondrial cytochrome oxidase subunit I (mtCOI) gene to study population structure in *H. longicornis*. However, PCR amplification of mtCOI with multiple species-specific primer pairs resulted in sequences containing long stretches of multiple peaks, suggesting co-amplification of a nuclear pseudogene in some, but not all, animals (~9% of specimens). Clean forward and/or reverse sequences were obtained for 65 specimens using the species-specific primers COI\_F1 (5' –CGT CTT GAA TTA GGG CAA CC – 3') and COI\_R1 (5' – AGM CCA ATT GCT AGC ATG GC – 3'), which were developed from a longer fragment of mtCOI that was amplified with universal calanoid primers L1384-COI and H2612-COI (Machida et al. 2004). We used these 65 sequences to compare the levels of genetic diversity in mtCOI and mtCOII for the same specimens, in order to place our work in context relative to other studies that use mtCOI as the primary genetic marker.

### *Sequence data analyses*

All forward and reverse mtCOII sequences were aligned using Multiple Sequence Comparison by Log-Expectation (MUSCLE) within Geneious Pro version 5.1.6 (Edgar 2004), checked for sequencing errors, and trimmed to a length of 546 bp. Unique haplotypes were identified (Collapse 1.2; Posada 2004; GenBank accession No. KC713636 - KC713781), and then translated to amino acid sequences using the invertebrate mitochondrial genetic code. Tajima's D was calculated for each collection site, as well as for all sites combined within each ocean gyre, to test for neutral evolution of mtCOII (Arlequin version 3.5; Excoffier and Lischer 2010).

The nucleotide substitution model that best fit our data was identified using the Akaike Information Criterion (jModelTest version 0.1.1, with default settings; Posada 2008), and TIM3+ with a gamma ( $\gamma$ ) of 0.305 was selected as the best model. However, since this model was not available in Arlequin (version 3.5), we used the most similar available model, Tamura and Nei with  $\gamma = 0.305$ , to perform genetic diversity tests and analyses of molecular variance (AMOVA; *see below*). To examine genetic diversity for each collection site, we calculated the number of alleles (HP-Rare 1.1; Kalinowski 2005), haplotype diversity, and nucleotide diversity (Arlequin version 3.5). A statistical parsimony network was generated using median-joining to identify relationships between haplotypes and examine the spatial distribution of haplotypes (Network 4.610, Network Publisher 1.3.0.0; Bandelt et al. 1999).

Population pairwise  $F_{ST}$  and  $\Phi_{ST}$  values were calculated to determine the genetic divergence between each pair of sites, but since they yielded the same conclusions, only  $F_{ST}$  values are reported here (Arlequin version 3.5; Excoffier and Lischer 2010).  $F_{ST}$  quantifies the genetic variation among subpopulations within the total population. The genetic diversity index  $D_{est}$  also was used to investigate genetic differentiation between collection sites (Software for the Measurement of Genetic Diversity (SMOGD) version 1.2.5; Crawford 2010), as this index accounts for the mean within-population heterozygosity observed in populations (Bird et al. 2011). To further investigate genetic differentiation between populations and to identify groups of samples that were genetically similar, we ran Principal Coordinates Analyses (PCoA) based on pairwise  $F_{ST}$  values, and inferred a population graph based on haplotype frequencies (Genetic Studio; Dyer 2009). Additionally, we ran three AMOVAs: 1) to test genetic divergence between groups on a global scale, using the groups identified with PCoA and population graphs, 2) to test for a genetic break in equatorial waters of the Atlantic Ocean, with northern and southern

Atlantic sites grouped (tropical sites included with the South Atlantic, *see* explanation in Results), and 3) to test for a genetic break in equatorial waters of the Pacific Ocean, with northern and southern sites grouped.

Another aim of this study was to test for isolation by distance (IBD) within and between subtropical gyres in the Atlantic and Pacific Oceans. Geographic distance between collection sites was calculated along a great circle route (the shortest distance between two points on the geoid; Matlab version R2012a) and then transformed non-linearly by calculating the logarithm of geographic distance ( $\log(\text{geographic distance})$ ), because the samples were collected over a two-dimensional area (Rousset 1997). Linearized  $F_{ST}$  was used as an estimate of genetic distance between site pairs (linearized  $F_{ST} = (F_{ST}/(1 - F_{ST}))$ ; Rousset 1997). We tested for isolation by distance by calculating the covariance of the genetic and geographic distance matrices for comparisons made within and between subtropical gyres in the Atlantic and Pacific Oceans (Mantel test; Arlequin version 3.5). To further characterize the relationship between genetic and geographic distance estimates, we regressed linearized  $F_{ST}$  on  $\log(\text{geographic distance})$  for all comparisons (linear regression).

Finally, because mtCOII is not a commonly used mitochondrial marker for population genetic studies, we compared genetic diversity at mtCOI (a more commonly used marker) and mtCOII for the same specimens, in order to understand how use of this marker may influence our perception of genetic diversity and structure in this species. Because some measures of genetic differentiation (i.e.,  $F_{ST}$  and its analogs) are influenced by the level of within-population heterozygosity of genetic markers (Wright 1978; Charlesworth 1998), large differences in diversity levels for mtCOII vs. mtCOI could indicate that our analyses using mtCOII are not comparable to other studies using mtCOI. In order to investigate genetic diversity at mtCOI and

mtCOII, sequences were obtained from both genes for six specimens from the North Pacific and 59 specimens from the South Pacific ( $n = 65$  total). These sequences were edited in Geneious Pro 5.1.6 and the alignment was trimmed to a length of 552 bp. Both forward and reverse sequences were available for 14 of these animals; single-strand sequences of mtCOI from the other 51 specimens also were included. The number of unique haplotypes and variable sites were identified with Collapse version 1.2 (Posada 2004), and compared between loci.

#### *Oceanographic sampling and analysis – Atlantic Ocean*

Oceanographic data and plankton samples from a basin-scale transect in the Atlantic Ocean (AMT20) were used to characterize the oceanographic habitat of *H. longicornis*. Along this cruise, conductivity temperature depth (CTD) casts were conducted at 89 sites to obtain vertical profiles of seawater temperature, salinity, density, chlorophyll *a*, oxygen concentration, down-welling photosynthetically active radiation (PAR), upwelling PAR, transmittance, light attenuation, and conductivity. The maximum depth of the casts varied from 300 –1000 m. Sensor calibration and data processing were handled by the Atlantic Meridional Transect programme (and British Oceanographic Data Centre, BODC). We focus here on seawater temperature and chlorophyll *a* profiles to detect large-scale ocean biomes and major gradients in biotic and abiotic ocean properties. Data were obtained from two replicate temperature and conductivity sensors as well as two in situ fluorometers (Sea-Bird Electronics (SBE) 3P Temperature Sensor; Chelsea MKIII Aquatracka Fluorometer). For each variable, data from both sensors were examined for errors, but measurements were used from only one sensor. Data points that were clearly erroneous (i.e., negative values) were omitted. Vertical profiles of temperature and chlorophyll *a* concentration were plotted against latitude for the entire length of

the AMT cruise (Ocean Data View 4.4.4; Schlitzer 2012), with data smoothed using Data-Interpolating Variational Analysis (DIVA) gridding to extrapolate over missing data points. In order to obtain data on abundance of *H. longicornis* across ocean biomes in the Atlantic, adult female *H. longicornis* were enumerated in every plankton sample collected on the AMT20 cruise ( $n = 33$ ).

## Results

mtCOII sequences were obtained for a total of 1059 specimens, with an average of ~26 animals per collection site (range 14 – 37; Table 1). Thirty-four of these sequences were obtained from specimens collected in tropical Atlantic stations, AMT20-17 to 20, where sample sizes were relatively small and PCR failure rate was high, potentially indicating that specimens in this region were dead or in poor condition upon collection (excluded from Table 1). There were 125 variable nucleotide sites in the mtCOII alignment, with no insertions or deletions. A total of 146 unique haplotypes were identified. Of the 125 polymorphic nucleotide sites, 32 also were variable in the translated amino acid sequences. A total of 47 unique amino acid sequences were sampled, and none of these sequences contained stop codons. Despite the relatively high number of amino acid substitutions, we infer that a functional copy of mtCOII was amplified because 1) the majority of nucleotide substitutions were synonymous (70%), 2) the translated sequences for *H. longicornis* aligned without gaps to the amino acid sequence for another calanoid species (71% similarity to *Eucalanus bungii*, Machida et al. 2004), and 3) similar variability has been observed at mtCOII in other arthropods (e.g., 20:82 variable amino acid sites in *Orchesella cincta*, Timmermans et al. 2005).

Tajima's D was statistically significant at only three sites (Table 1; Sites 32, 33, and 38;  $p \leq 0.05$  for all), and was non-significant for all ocean gyres ( $p > 0.05$  for all, samples within gyres pooled), suggesting a stable demographic history for these populations and neutral evolution of mtCOII (Wares 2010). mtCOII haplotype diversity ( $h$ ) ranged from 0.48 to 0.97 (median = 0.80), allelic richness ( $R_d$ ) ranged from 4.15 to 11.75 (median = 7.44), and nucleotide diversity ( $\pi$ ) ranged from 0.0079 to 0.0264 (median = 0.0200). The Indian Ocean and South Atlantic collection sites had significantly higher haplotype diversity and allelic richness than the North Pacific and the North Atlantic (analysis of variance (ANOVA);  $p < 0.05$  for all). Based on the

mtCOI and mtCOII sequences that were compared across the same 65 specimens, mtCOII had a comparable level of genetic variation as mtCOI. There were 33 variable sites and 17 unique haplotypes identified in the mtCOI sequences, and 41 variable sites and 18 unique haplotypes in the mtCOII sequences (all sequences 552 bp in length).

### *Global-scale patterns - Genetic structure*

A total of 146 unique haplotypes were sampled in this study, of which 42 were sampled more than once (i.e., were not singletons). Most haplotypes were only a few base pair substitutions away from their nearest neighbor, but there were two large breaks (6 and 7 bp mutations) that separated the haplotypes into three groups (Fig. 2). However, these groups were not geographically defined. Comparisons between ocean gyre systems revealed that most non-singleton haplotypes were observed in more than one gyre, and genetic structure in *H. longicornis* was driven primarily by changes in haplotype frequency rather than presence or absence of haplotypes (Figs. 2, 3, 4A, B). Four non-singleton private haplotypes were restricted to one gyre (e.g., H3 in the Indian Ocean; H45, H49, and H66 in the North Atlantic), and three haplotypes were globally distributed (e.g. H5, H9, and H18). The most common haplotype (H10;  $n = 174$ ) was found predominantly in the North Atlantic but was sampled in every other gyre except for the North Pacific.

The four samples from the Atlantic equatorial region (AMT20 – 17 to 20, 2.0-10.6° N) had a total of 23 haplotypes (shown in Fig. 2 but not in Fig. 4 due to small sample sizes, *see* above). Of these 23 haplotypes, eleven were sampled elsewhere in the Atlantic (and in most cases, in both the northern and southern hemispheres), one was only sampled at two sites in the Indian and the South Pacific, and eleven were not sampled at any other site around the globe.

Pairwise  $F_{ST}$  values ranged from -0.022 to 0.46 (median = 0.13), with 56% of comparisons significant following a strict Bonferroni correction (pairwise  $\alpha = 0.000067$ , significant pairwise  $F_{ST} = 0.055 - 0.46$ ; underlined in Table 2). An additional 29% of comparisons had  $p$ -values between 0.05 and 0.000067, but were non-significant using the stringent pairwise  $\alpha$  in Bonferroni correction ( $F_{ST} = 0.025 - 0.165$ ; shown in bold, Table 2). Generally, pairwise  $F_{ST}$  values were lower (and often non-significant) for comparisons made within rather than between ocean gyre systems (within gyres:  $F_{ST} = -0.022 - 0.28$ , median = 0.022; between gyres:  $F_{ST} = -0.021 - 0.46$ , median = 0.15). Many non-significant  $F_{ST}$  values were observed among sites in the Indian Ocean, South Atlantic, and tropical North Atlantic. Overall, results of  $D_{est}$  analyses were similar to  $F_{ST}$  analyses ( $D_{est} = -0.043 - 0.299$ , median = 0.091), which lends confidence to our interpretation of patterns of genetic structure (Bird et al. 2011).  $D_{est}$  and pairwise  $F_{ST}$  values were highest (median: 0.166 and 0.237, respectively) and all pairwise  $F_{ST}$  values were significant ( $p < 0.01$  for all) for comparisons between the North Pacific and North Atlantic sites.

PCoA (Fig. 5) and population graph analyses (Fig. S1) both showed strong genetic divergence between four groups of populations: (1) South Pacific, (2) North Pacific, (3) North Atlantic populations (including the Mediterranean Sea, Site 39), and (4) Indian Ocean, tropical North Atlantic (Sites 27 and 28; see explanation below), and the South Atlantic populations. An analysis of molecular variance (AMOVA) with this hierarchical population structure resulted in a global  $F_{ST}$  of 0.20, with ~15% of the variation occurring among groups, ~5% within groups, and ~80% within sites ( $F_{CT} = 0.15$ ,  $F_{SC} = 0.06$ ;  $p < 0.00001$  for all fixation indices, where  $F_{CT}$  and  $F_{SC}$  measure genetic divergence among groups and among populations within each group, respectively). Although the western tropical North Atlantic sites are in the northern hemisphere,

the two sites nearest the equator (Sites 27 and 28; 3.6°N and 9.6° N; Table 1) were genetically more similar to the South Atlantic sites (Fig. 4A).

### *Genetic breaks in tropical oceans*

Strong genetic structure was observed between northern and southern hemispheres in both the Atlantic and Pacific Oceans. An AMOVA was used to test the hypothesis of genetic breaks occurring in equatorial waters of both the Atlantic and Pacific Oceans. In this analysis, the hierarchical structure was defined using population graph (Fig. S1) and PCoA results (Fig. 5), with collection sites divided into groups separated along the equator, with the exception that two of the western tropical North Atlantic sites (Sites 27 and 28; Table 1) were grouped with the South Atlantic (Table 2; Fig 4A). In the Atlantic Ocean, ~21% of the genetic variation occurred among hemispheres, and ~77% and ~2% of the variation occurred within and among sites, respectively ( $p < 0.00001$  for all fixation indices; Table 3). In the Pacific Ocean, a slightly smaller percentage of genetic variation occurred among hemispheres (~15%), and slightly more variation occurred within and among sites (~79% and ~5%, respectively;  $p < 0.00001$  for all fixation indices).

No pattern of isolation by distance (IBD) was found among sites within each of the four subtropical gyres of the Atlantic and Pacific Oceans (Mantel tests; linear regression:  $R^2 = 0.0593$  for North Pacific,  $R^2 = 0.0674$  for South Pacific,  $R^2 = 0.0001$  for North Atlantic,  $R^2 = 0.0529$  for South Atlantic;  $p \gg 0.05$  for all; Fig. 6). However, when basin-wide comparisons were made, there was significant support for IBD in both the Atlantic and the Pacific ( $p < 0.01$  for Mantel; linear regression:  $R^2 = 0.142$  for Pacific,  $R^2 = 0.266$  for Atlantic;  $p < 0.001$  for both; Fig. 7). The

significant result for IBD at the basin scale is likely driven by the genetic break observed in the equatorial region in both ocean basins (Fig. 5).

#### *Ocean habitat of Haloptilus longicornis*

The 2010 AMT20 cruise transited across all major pelagic biomes in the Atlantic Ocean, including cold, nutrient-rich subpolar waters, oligotrophic subtropical gyres, and upwelled equatorial waters (Fig. 4D, E). The cold, well-mixed subpolar waters ( $>35^{\circ}\text{N}$  and  $>30^{\circ}\text{S}$ ) were characterized by shallow ( $<100$  m) and high ( $0.2\text{-}1\text{ mg m}^{-3}$ ) maximum chlorophyll concentrations, while the subtropical gyres ( $12\text{-}35^{\circ}\text{N}$ ,  $0\text{-}30^{\circ}\text{S}$ ) were characterized by a deep thermocline (150-300 m) and very low chlorophyll concentrations ( $<0.2\text{ mg m}^{-3}$ ) at a deep chlorophyll maximum ( $\sim 100\text{-}150$  m). The equatorial region ( $\sim 0\text{-}12^{\circ}\text{N}$ ) had a shallower chlorophyll maximum (50-100 m) than the subtropical gyres, and moderate chlorophyll concentrations ( $0.3\text{-}0.5\text{ mg m}^{-3}$ ; Fig. 4D, E).

*Haloptilus longicornis* showed a bimodal pattern of abundance in the Atlantic Ocean, with high abundance within the subtropical gyres of both the northern and southern hemispheres and low abundance in both subpolar regions and equatorial waters (Fig. 4C). Within the subtropical gyre ecosystems, the mean abundance of 932 adult females per  $1000\text{ m}^3$  water (range: 220-2347) was significantly greater than abundances in equatorial waters ( $\sim 0\text{-}12^{\circ}\text{N}$ ; mean = 270, range: 173-413;  $t$ -test,  $t = -2.31$ , degrees of freedom ( $df$ ) = 20,  $p = 0.03$ ). The northern and southern distributional boundaries for this species occur near  $35^{\circ}\text{N}$  and  $30^{\circ}\text{S}$ , as evidenced by abundance dropping to  $\sim 0\text{-}210$  adult females per  $1000\text{ m}^3$  seawater (median:  $\sim 13$ ) poleward of these latitudes, with the species disappearing altogether by  $>49^{\circ}\text{N}$  and  $>39^{\circ}\text{S}$ . It is important to note that the sampling depth was decreased from 300 m to 200 m as the cruise

continued south past 12°S (Sites 22-24, Table 1), and given the predominantly mesopelagic depth habitat of this species, the 200 m depth of sampling likely overlaps only the upper portion of the depth range of the species. This change in sampling depth therefore may explain the decrease in *H. longicornis* abundance seen south of 12°S (Sites 22-24), relative to the abundances observed in the northern subtropical gyre (Fig. 4C).

## Discussion

### *Dispersal barriers in the open sea*

Prior molecular work on marine holozooplankton has shown that genetic structure among populations is often quite high, despite early expectations that these populations would be genetically homogeneous (Papetti et al. 2005; Chen and Hare 2011; Goetze 2011). However, very few studies have been conducted on oceanic species, and in many cases the spatial scale of sampling has been small relative to the species' distributional ranges. For this reason, little information is available on oceanic dispersal barriers for holoplanktonic taxa. The geographic coverage of this study was extensive in comparison to prior work, and allowed us to detect strong genetic breaks between subtropical gyre populations in the northern and southern hemispheres of both the Atlantic and Pacific Oceans in the mesopelagic copepod *H. longicornis*. Results from principal coordinates, population graph, IBD and AMOVA analyses, as well as population pairwise  $F_{ST}$  values, all supported the inference of strong genetic structure across equatorial waters in both the Pacific and Atlantic Oceans. The population genetic break in the Atlantic coincided with decreased abundance in equatorial waters, suggesting the presence of an open-ocean dispersal barrier for this species. This is one of the first such oceanographic dispersal barriers reported for oceanic holoplankton.

Despite the strong structuring across equatorial waters in the Atlantic, *H. longicornis* was continuously present in low abundance throughout this region. The genetic composition of this equatorial population was complex, and it is challenging to identify the exact location of the genetic break, in part due to low abundance. The tropical North Atlantic material that was collected near the western boundary (Sites 27 and 28) was genetically more similar to the South Atlantic than the other North Atlantic populations. This genetic pattern may be driven by the

North Brazil Current (NBC), with migration occurring in stochastic eddies that move from the southern to the northern hemisphere along the western boundary (Schott et al. 1998). The equatorial genetic break likely occurs slightly north of the equator across the entire Atlantic basin, within the Western Tropical Atlantic province ( $\sim 13^{\circ}\text{N}$  -  $\sim 5^{\circ}\text{S}$ , Longhurst 2007), which is thought to be poor habitat for *H. longicornis* (see below). Nearly half of the specimens collected at tropical Atlantic sites shared haplotypes with northern and/or southern Atlantic populations, and the individuals in this region may be expatriates from the subtropical gyres. Collection of more specimens in the equatorial region of both the Atlantic and Pacific Oceans may help clarify the complex genetic composition of these populations.

Abundance data for *H. longicornis* provided insight into the large-scale biogeography of this species and the possible mechanisms underlying the dispersal barrier in the Atlantic Ocean. Atlantic plankton samples (AMT20) were collected from ocean provinces in the North Atlantic Subtropical Gyre (NAST;  $\sim 41^{\circ}\text{N}$  -  $\sim 27^{\circ}\text{N}$ ), North Atlantic Tropical Gyre (NATR;  $\sim 27^{\circ}\text{N}$  -  $\sim 13^{\circ}\text{N}$ ), Western Tropical Atlantic (WTRA;  $\sim 13^{\circ}\text{N}$  -  $\sim 5^{\circ}\text{S}$ ), and the South Atlantic Gyre (SATL;  $\sim 5^{\circ}\text{S}$  -  $\sim 35^{\circ}\text{S}$ ), as defined by Longhurst (2007). Large-scale shifts in the dominance and diversity of a number of planktonic groups are well-known to occur across these ocean biomes that coincide with our observed spatial changes in the abundance of *H. longicornis* (Schattenhofer et al. 2009; Schnack-Schiel et al. 2010). *Haloptilus longicornis* was much more abundant in the subtropical gyres of the Atlantic ( $\sim 30^{\circ}\text{S}$ ,  $\sim 12^{\circ}\text{N}$ - $35^{\circ}\text{N}$ ; SATL, NAST, NATR provinces), and these are clearly the preferred habitat for the species. The species was present, but rare, in equatorial waters ( $\sim 0^{\circ}\text{N}$ - $12^{\circ}\text{N}$ ; WTRA province), and we hypothesize that this region provides suboptimal habitat for survival and/or reproduction of this species. Thus, we think it

unlikely that individuals in this region constitute a true stepping-stone population for migrants dispersing among gyres.

Given these new insights into the biogeography of this species (above; compare to Razouls et al. 2005-2012), either physical or biophysical mechanisms may underlie the equatorial dispersal barrier for *H. longicornis*. Zonal currents in the equatorial region of the Atlantic, including the Equatorial Currents and Undercurrents (North, South), may restrict dispersal of organisms between hemispheres by advecting them parallel to the equator into coastal waters, and out of suitable pelagic habitat (an exclusively physical barrier). Alternatively, a more complex biophysical barrier may occur in equatorial waters, due to unsuitability of habitat and altered population dynamics for *H. longicornis* in this region. Under this hypothesis, poor quality habitat in equatorial waters would cause higher mortality or lower reproductive rates of migrants traveling between subtropical gyres, and/or prevent the establishment of intermediate (stepping-stone) populations. Migrants traveling along the western boundary in the NBC also may be exposed to lower salinity and higher nutrient waters from the Amazon outflow, which is known to create a strong dispersal barrier for reef fishes (the Amazon barrier, *see* below; Rocha et al. 2007)

Genetic breaks in equatorial waters have been reported for a number of other marine species, with diverse possible mechanisms proposed to underlie the observed population structure. Atlantic equatorial genetic breaks have been observed in coastal, demersal species along the southwestern Atlantic coast (e.g., spiny lobster, *Panulirus argus*, Sarver et al. 1998; reef fishes, Rocha et al. 2007), and are thought to be linked to high freshwater and sediment discharge from the Amazon river that isolates coastal marine habitats on either side of the freshwater plume. Pelagic species with continuous tropical – subtropical distributions also have

been found to have equatorial genetic breaks (e.g., Atlantic swordfish, *Xiphias gladius*, Chow et al. 2007; white marlin, *Tetrapturus albidus*, Graves and McDowell 2006), but the causes of these breaks are not well understood. Chow et al. (2007) speculated that the genetic break in swordfish was maintained by isolated spawning grounds, low migration rates of adults, and low connectivity of planktonic larvae across the equator, which may be driven by spatial gradients in oceanographic conditions. In the holoplankton, only Goetze (2011) has previously reported a genetic break in the equatorial Atlantic, but Atlantic sampling was limited in this study, and possible mechanisms were not fully explored. Although the number of studies reporting equatorial genetic breaks for pelagic species is relatively few, this genetic pattern may occur more often than has been reported, because spatially comprehensive sampling across open ocean habitats is required to detect these large-scale genetic patterns.

#### *Global-scale patterns of genetic structure*

Strong genetic structure also was observed between ocean basins in *H. longicornis*, with the exception of low genetic divergence between the Indian, South Atlantic, and tropical North Atlantic populations. The strong structure found between the North Atlantic; North Pacific; South Pacific; and Indian and South Atlantic suggests that populations in these regions likely do not exchange migrants contemporarily, although coalescent analyses with multi-locus data are needed to confirm this inference (Marko and Hart 2011). Genetic divergence between populations in the Atlantic and Pacific Oceans is commonly observed in marine species, including nekton (Alvarado Bremer et al. 2005; Rocha et al. 2007) and zooplankton (Goetze 2005, 2011; Blanco-Bercial et al. 2011), and is usually attributed to land mass barriers in tropical and subtropical latitudes that effectively isolate these ocean provinces from one another.

For *H. longicornis*, there appears to be a significant barrier to dispersal between the Indian and Pacific Oceans as well, despite the absence of a continental landmass separating these oceans. Genetic divergence between Indian and Pacific populations has been reported in many other tropical and subtropical species, including reef-associated vertebrates and invertebrates (e.g., reef fishes reviewed by Rocha et al. 2007; gastropod *Nerita albicilla*, Crandall et al. 2008) as well as a few planktonic copepods (e.g., *Eucalanus hyalinus* and *E. spinifer*, Goetze 2005). For many species, high genetic structure across this region has been hypothesized to have arisen historically due to isolation of the Indian and Pacific Ocean basins during Pleistocene low sea level stands, during which extensive land and seasonal upwelling barriers effectively prevented dispersal across the Sunda shelf (Fleminger 1986; Nelson et al. 2000). Although there is not a contiguous land barrier in the Indo-Pacific in the contemporary ocean, genetic divergence between Indian and Pacific *H. longicornis* populations may be maintained by low contemporary dispersal. Because most of the seafloor in this region is relatively shallow (<200 m) and *H. longicornis* live in the upper-mesopelagic zone, there are only a few narrow passageways through which these animals can disperse between oceans (Gordon 2005). Differences between planktonic species (e.g., *P. xiphias* and *H. longicornis*) in the observed patterns of genetic structure across this region may indicate that species-specific habitat depth plays an important role in dispersal among basins (Goetze 2011; this study). For example, *H. longicornis* lives in the ~100-400 m depth range and exhibits a sharp genetic break across the Indo-Pacific region. In contrast, *P. xiphias*, which also occurs in the mesopelagic zone during the daytime (200-1000 m), but migrates vertically and is present in surface waters at night, was found to have low genetic structure across populations in the western Pacific and eastern Indian Oceans. These results suggest high connectivity for this species across the Sunda Shelf via dispersal in surface

currents (Goetze 2011). Comparative studies of plankton species with distinct habitat depths would be informative regarding how species-specific depth preferences influence the strength of this Indo-Pacific dispersal barrier.

A lack of genetic structure was found between *H. longicornis* populations in the South Atlantic, Tropical North Atlantic, and Indian Oceans. Multiple processes could explain this pattern (Goetze 2005). This absence of genetic structure may occur due to contemporary migration between Atlantic and Indian Ocean populations, as has been reported for some fishes and sharks (Brendtro et al. 2008; Daly-Engel et al. 2012). An alternative hypothesis is that these populations experienced migration historically, and a barrier to dispersal has arisen only recently between these ocean basins. Given large effective population size ( $N_e$ ; Bucklin and Wiebe 1998; Peijnenburg et al. 2005), these populations may not have been isolated for a sufficiently long period of time for genetic divergence to accrue. It is also possible that we have detected a range expansion from one ocean basin to another, which has been inferred for some fish species (Rocha et al. 2005; Bowen et al. 2006). Further studies using coalescent analyses on multi-locus data are needed to differentiate between these hypotheses.

Finally, one of the recurring patterns observable in our data across the global ocean was the lack of genetic subdivision among collection sites within subtropical gyres. Low or non-significant pairwise  $F_{ST}$  values were found for within-gyre comparisons in four replicate subtropical gyres (North and South Pacific, North and South Atlantic; Table 2), in addition to non-significant within-gyre IBD results (Fig. 6). Similar patterns have been reported in other holoplanktonic taxa (Goetze 2005, 2011; *Clausocalanus lividus*, Blanco-Bercial et al. 2011), but this study provides the most spatially comprehensive demonstration of this pattern to date.

These results were as predicted for this species, given that *H. longicornis* is expected to be entrained in near-surface gyre currents due to its upper-mesopelagic habitat.

In conclusion, most research on marine dispersal barriers has focused on coastal and reef-associated species, and dispersal barriers are not yet well defined for pelagic holoplankton. In this study, we found genetic breaks for *H. longicornis* between most ocean basins and in the equatorial regions of both the Atlantic and Pacific Oceans. Although the causes of the equatorial genetic breaks are currently unknown, oceanographic data and abundance measurements for *H. longicornis* from the Atlantic Ocean indicate that the equatorial region may be poor quality habitat for this species and may impede dispersal among subtropical gyres. Given that other holoplanktonic species also show a bimodal pattern of abundance across the subtropics and tropics (e.g., *Clausocalanus paululus*, *C. parapergens*, Schnack-Schiel et al. 2010), it is likely that the equatorial region serves as a dispersal barrier for other members of the holoplankton community. Community-wide genetic studies need to be conducted at basin spatial scales to fully understand the prevalence and importance of these open-ocean dispersal barriers for the holozooplankton.

## References Cited

- Alberto, F., P. T. Raimondi, D. C. Reed, N. C. Coelho, R. Leblois, A. Whitmer, and E. A. Serrao. 2010. Habitat continuity and geographic distance predict population genetic differentiation in giant kelp. *Ecology* **91**: 49–56.
- Alvarado Bremer, J. R., J. Mejuto, J. Gómez-Márquez, F. Boán, P. Carpintero, J. M. Rodríguez, J. Viñas, T. W. Greig, and B. Ely. 2005. Hierarchical analyses of genetic variation of samples from breeding and feeding grounds confirm the genetic partitioning of northwest Atlantic and South Atlantic populations of swordfish (*Xiphias gladius* L.). *J. Exp. Mar. Biol. Ecol.* **327**: 167–182.
- Ambler, J. W., and C. Miller. 1987. Vertical habitat-partitioning by copepodites and adults of subtropical oceanic copepods. *Mar. Biol.* **94**: 561–577.
- Bandelt, H.-J., P. Forster, and A. Röhl. 1999. Median-joining networks for inferring intraspecific phylogenies. *Mol. Biol. Evol.* **16**: 37–48.
- Baums, I. B., C. B. Paris, and L. M. Chérubin. 2006. A bio-oceanographic filter to larval dispersal in a reef-building coral. *Limnol. Oceanogr.* **51**: 1969–1981.
- Bird, C. E., S. A. Karl, P. E. Smouse, and R. J. Toonen. Detecting and measuring genetic differentiation, p. 31–55. *In* S. Koenemann, C. Held and C. Schubart [eds.], *Phylogeography and population genetics in Crustacea*. CRC Press.
- Blanco-Bercial, L., F. Álvarez-Marqués, and A. Bucklin. 2011. Comparative phylogeography and connectivity of sibling species of the marine copepod *Clausocalanus* (Calanoida). *J. Exp. Mar. Biol. Ecol.* **404**: 108–115.

- Bowen, B. W., A. Muss, L. A. Rocha, and W. S. Grant. 2006. Shallow mtDNA coalescence in Atlantic pygmy angelfishes (Genus *Centropyge*) indicates a recent invasion from the Indian Ocean. *J. Hered.* **97**: 1–12.
- Bradford-Grieve, J. 1999. The marine fauna of New Zealand: Pelagic calanoid Copepoda: Bathypontiidae, Arietellidae, Augaptilidae, Heterorhabdidae, Lucicutiidae, Metridinidae, Phyllopodidae, Centropagidae, Pseudodiaptomidae, Temoridae, Candaciidae, Pontellidae, Sulcanidae, Acartiidae, Tortanidae. National Institute of Water and Atmospheric Research.
- Brendtro, K. S., J. R. McDowell, and J. E. Graves. 2008. Population genetic structure of escolar (*Lepidocybium flavobrunneum*). *Mar. Biol.* **155**: 11–22.
- Bucklin, A., S. Kaartvedt, M. Guarnieri, and U. Goswami. 2000. Population genetics of drifting (*Calanus* spp.) and resident (*Acartia clausi*) plankton in Norwegian fjords. *J. Plankton Res.* **22**: 1237–1251.
- Bucklin, A., and P. H. Wiebe. 1998. Low mitochondrial diversity and small effective population sizes of the copepods *Calanus finmarchicus* and *Nannocalanus minor*: Possible impact of climate variation during recent glaciation. *The American Genetic Association* **89**: 383–392.
- Charlesworth, B. 1998. Measures of divergence between populations and the effect of forces that reduce variability. *Mol. Biol. Evol.* **15**: 538–543.
- Chen, G., and M. P. Hare. 2011. Cryptic diversity and comparative phylogeography of the estuarine copepod *Acartia tonsa* on the US Atlantic coast. *Mol. Ecol.* **20**: 2425–2441.

- Chow, S., S. Clarke, M. Nakadate, and M. Okazaki. 2007. Boundary between the north and south Atlantic populations of the swordfish (*Xiphias gladius*) inferred by a single nucleotide polymorphism at calmodulin gene intron. *Mar. Biol.* **152**: 87–93.
- Claus, C. 1863. Die frei lebenden Copepoden mit besonderer Berücksichtigung der Fauna Deutschlands, der Nordsee und des Mittelmeeres. W. Engelmann. [The free-living copepods, with special consideration of the German, North Sea, and Mediterranean fauna.]
- Cowen, R. K., and S. Sponaugle. 2009. Larval dispersal and marine population connectivity. *Annu. Rev. Mar. Sci.* **1**: 443–466.
- Crandall, E. D., M. A. Frey, R. K. Grosberg, and P. H. Barber. 2008. Contrasting demographic history and phylogeographical patterns in two Indo-Pacific gastropods. *Mol. Ecol.* **17**: 611–626.
- Crawford, N. G. 2010. SMOGD: software for the measurement of genetic diversity. *Mol. Ecol. Resour.* **10**: 556–557.
- Cronin, T. W., and R. B. Forward, Jr. 1986. Vertical migration cycles of crab larvae and their role in larval dispersal. *Bull. Mar. Sci.* **39**: 192–201.
- Daly-Engel, T. S., K. D. Seraphin, K. N. Holland, J. P. Coffey, H. A. Nance, R. J. Toonen, and B. W. Bowen. 2012. Global phylogeography with mixed-marker analysis reveals male-mediated dispersal in the endangered scalloped hammerhead shark (*Sphyrna lewini*). *PLoS ONE* **7**: e29986, doi:10.1371/journal.pone.0029986
- Dyer, R. J. 2009. GeneticStudio: A suite of programs for spatial analysis of genetic-marker data. *Mol. Ecol. Resour.* **9**: 110-113.

- Edgar, R. C. 2004. MUSCLE: a multiple sequence alignment method with reduced time and space complexity. *BMC Bioinf.* **5**: 113.
- Excoffier, L., and H. E. L. Lischer. 2010. Arlequin suite version 3.5: A new series of programs to perform population genetics analyses under Linux and Windows. *Mol. Ecol. Resour.* **10**: 564–567.
- Fleminger, A. 1986. The Pleistocene equatorial barrier between the Indian and Pacific oceans and a likely cause for Wallace's Line, p. 84-97. *In* A. C. Pierrot-Bults, S. Van der Spoel, B. J. Zahuranec and R. K. Johnson [eds.], UNESCO Technical Papers in Marine Science 49.
- Gerlach, G., J. Atema, M. J. Kingsford, K. P. Black, and V. Miller-Sims. 2007. Smelling home can prevent dispersal of reef fish larvae. *Proc. Natl. Acad. Sci. U. S. A.* **104**: 858–863.
- Goetze, E. 2005. Global population genetic structure and biogeography of the oceanic copepods *Eucalanus hyalinus* and *E. spinifer*. *Evolution* **59**: 2378–2398.
- Goetze, E. 2011. Population differentiation in the open sea: Insights from the pelagic copepod *Pleuromamma xiphias*. *Integr. Comp. Biol.* **51**: 580–597.
- Gordon, A. L. 2005. Oceanography of the Indonesian Seas and their throughflow. *Oceanography* **18**: 14–27.
- Graves, J. E., and J. R. McDowell. 2006. Genetic analysis of white marlin (*Tetrapturus albidus*) stock structure. *Bull. Mar. Sci.* **79**: 469–482.
- Johnson, M. S., and R. Black. 1995. Neighbourhood size and the importance of barriers to gene flow in an intertidal snail. *Heredity* **75**: 142–154.
- Kalinowski, S. T. 2005. HP-RARE 1.0: a computer program for performing rarefaction on measures of allelic richness. *Mol. Ecol. Notes* **5**: 187–189.

- Longhurst, A. R. 2007. Ecological geography of the sea. Academic Press.
- Machida, R. J., M. U. Miya, M. Nishida, and S. Nishida. 2004. Large-scale gene rearrangements in the mitochondrial genomes of two calanoid copepods *Eucalanus bungii* and *Neocalanus cristatus* (Crustacea), with notes on new versatile primers for the srRNA and COI genes. *Gene* **332**: 71–78.
- Marko, P. B., and M. W. Hart. 2011. The complex analytical landscape of gene flow inference. *Trends Ecol. Evol.* **26**: 448–456.
- McGowan, J. A., and P. W. Walker. 1979. Structure in the copepod community of the North Pacific central gyre. *Ecol. Monogr.* **49**: 195–226.
- Mori, T. 1964. The pelagic Copepoda from the neighbouring waters of Japan. The Soyo Company.
- Nelson, J. S., R. J. Hoddell, L. M. Chou, W. K. Chan, and V. P. E. Phang. 2000. Phylogeographic structure of false clownfish, *Amphiprion ocellaris*, explained by sea level changes on the Sunda shelf. *Mar. Biol.* **137**: 727–736.
- Norris, R. D. 2000. Pelagic species diversity, biogeography, and evolution. *Paleobiology* **26**: 236–258.
- Papetti, C., L. Zane, E. Bortolotto, A. Bucklin, and T. Patarnello. 2005. Genetic differentiation and local temporal stability of population structure in the euphausiid *Meganyctiphanes norvegica*. *Mar. Ecol. Prog. Ser.* **289**: 225–235.
- Peijnenburg, KTCA., E. K. van Haastrecht, and C. Fauvelot. 2005. Present-day genetic composition suggests contrasting demographic histories of two dominant chaetognaths of the North-East Atlantic, *Sagitta elegans* and *S. setosa*. *Mar. Biol.* **147**: 1279–1289.
- Posada, D. 2004. COLLAPSE 1.2. Free Software Foundation Incorporation Boston.

- Posada, D. 2008. jModelTest: phylogenetic model averaging. *Mol. Biol. Evol.* **25**: 1253–1256.
- Provan, J., G. E. Beatty, S. L. Keating, C. A. Maggs, and G. Savidge. 2009. High dispersal potential has maintained long-term population stability in the North Atlantic copepod *Calanus finmarchicus*. *Proc. R. Soc. Lond. B Biol. Sci.* **276**: 301–307.
- Razouls, C., F. de Bovee, J. Kouwenberg, and N. Desreumaux. 2005-2012. Diversity and geographic distribution of marine planktonic copepods. Available at <http://copepodes.obs-banyuls.fr/en> [Accessed 25 September 2012]
- Rocha, L. A., M. T. Craig, and B. W. Bowen. 2007. Phylogeography and the conservation of coral reef fishes. *Coral Reefs* **26**: 501–512.
- Rocha, L. A., D. R. Robertson, C. R. Rocha, J. L. van Tassell, M. T. Craig, and B. W. Bowen. 2005. Recent invasion of the tropical Atlantic by an Indo-Pacific coral reef fish. *Mol. Ecol.* **14**: 3921–3928.
- Rousset, F. 1997. Genetic differentiation and estimation of gene flow from *F*-statistics under isolation by distance. *Genetics* **145**: 1219–1228.
- Saraladevi, K., R. Stephen, and T. S. S. Rao. 1979. Distribution of *Haloptilus* (Copepoda, Calanoida) in the Indian Ocean. *Indian J. Mar. Sci.* **8**: 159–165.
- Sars, G. O. 1902. An account of the crustacea of Norway with short descriptions and figures of all the species. Bergen Museum.
- Sarver, S. K., J. D. Silberman, and P. J. Walsh. 1998. Mitochondrial DNA sequence evidence supporting the recognition of two subspecies or species of the Florida spiny lobster *Panulirus argus*. *J. Crustacean Biol.* **18**: 177–186.

- Schattenhofer, M., B. M. Fuchs, R. Amann, M. V. Zubkov, G. A. Tarran, and J. Pernthaler. 2009. Latitudinal distribution of prokaryotic picoplankton populations in the Atlantic Ocean. *Environ. Microbiol.* **11**: 2078–2093.
- Schlitzer, R. 2012. Ocean Data View, <http://odv.awi.de>
- Schnack-Schiel, S. B., E. Mizdalski, and A. Cornils. 2010. Copepod abundance and species composition in the Eastern subtropical/tropical Atlantic. *Deep-Sea Res. II* **57**: 2064–2075.
- Schott, F. A., J. Fischer, and L. Stramma. 1998. Transports and pathways of the upper-layer circulation in the Western tropical Atlantic. *J. Phys. Oceanogr.* **28**: 1904–1928.
- Timmermans, MJTN., J. Ellers, J. Mariën, S. C. Verhoef, E. B. Ferwerda, and N. M. van Straalen. 2005. Genetic structure in *Orchesella cincta* (Collembola): Strong subdivision of European populations inferred from mtDNA and AFLP markers. *Mol. Ecol.* **14**: 2017–2024.
- Wares, J. P. 2010. Natural distributions of mitochondrial sequence diversity support new null hypotheses. *Evolution* **64**: 1136–1142.
- White, C., K. A. Selkoe, J. Watson, D. A. Siegel, D. C. Zacherl, and R. J. Toonen. 2010. Ocean currents help explain population genetic structure. *Proc. R. Soc. Lond. B Biol. Sci.* **277**: 1685–1694.
- Wright, S. 1978. *Evolution and the genetics of populations, Vol. IV. Variability within and among natural populations.* University of Chicago Press.

## Tables

Table 1. Population samples and summary statistics for *Haloptilus longicornis*. Site - collection site number, Sample - cruise name and station number, n - number of individuals sequenced, H - number of haplotypes, h - haplotype diversity, Rd - allelic richness,  $\pi$  - nucleotide diversity, D - Tajima's D, with bold indicating significance at  $\alpha = 0.05$ , p - the probability that the simulated D is statistically the same as the observed D, and the final column lists the ocean basin and hemisphere within which the sample was collected. An additional 34 individuals were collected at four stations in the equatorial Atlantic (AMT20-17 to 20; 2-10oN), but they are not included here because of relatively low sample sizes (n = 5-15).

Site	Sample	Latitude	Longitude	n	H	h	R <sub>d</sub>	$\pi$	D	p	Ocean basin
1	VANC10MV-02	-35.067	24.502	28	20	0.97 +/- 0.02	11.75	0.0228 +/- 0.0118	0.0019	0.57	Indian
2	VANC10MV-06	-34.054	40.508	24	12	0.88 +/- 0.05	8.33	0.0200 +/- 0.0105	0.3874	0.71	Indian
3	VANC10MV-11	-29.850	59.844	25	10	0.80 +/- 0.08	7.18	0.0176 +/- 0.0093	0.4144	0.71	Indian
4	VANC10MV-17	-18.434	80.920	27	11	0.85 +/- 0.05	7.55	0.0187 +/- 0.0098	0.0862	0.59	Indian
5	VANC10MV-23	-12.219	96.787	26	17	0.96 +/- 0.02	10.85	0.0219 +/- 0.0114	-0.3015	0.43	Indian
6	VANC10MV-27	-16.580	115.379	25	13	0.93 +/- 0.03	9.26	0.0209 +/- 0.0109	-0.2545	0.45	Indian
7	COOK11MV-005	-2.237	145.222	21	13	0.91 +/- 0.05	9.54	0.0244 +/- 0.0128	0.4218	0.72	S Pacific
8	COOK07MV-001	14.529	145.087	27	6	0.74 +/- 0.06	4.97	0.0241 +/- 0.0125	1.2723	0.92	N Pacific
9	COOK11MV-002	18.194	132.443	25	12	0.80 +/- 0.08	7.57	0.0251 +/- 0.0130	0.3775	0.71	N Pacific
10	ACE ASIA 19	32.262	134.225	29	10	0.82 +/- 0.06	6.76	0.0264 +/- 0.0136	0.6537	0.80	N Pacific
11	ACE ASIA 13	32.751	154.926	26	6	0.66 +/- 0.06	4.15	0.0231 +/- 0.0120	2.1860	0.99	N Pacific
12	ACE ASIA 8	31.241	173.919	26	7	0.68 +/- 0.09	5.20	0.0220 +/- 0.0114	0.6234	0.78	N Pacific
13	ACE ASIA 2	28.207	-162.137	25	7	0.59 +/- 0.11	4.98	0.0200 +/- 0.0105	0.7382	0.82	N Pacific
14	HAWAIIAN WATERS	21.234	-158.158	37	12	0.77 +/- 0.06	6.59	0.0213 +/- 0.0110	-0.0261	0.56	N Pacific
15	S226-010-TT	13.083	-159.343	26	10	0.79 +/- 0.06	6.56	0.0262 +/- 0.0135	0.4639	0.74	N Pacific
16	COOK14MV-40	-14.107	-172.132	25	12	0.92 +/- 0.03	8.96	0.0200 +/- 0.0105	0.1566	0.62	S Pacific
17	COOK14MV-10	-23.502	-174.129	27	13	0.92 +/- 0.03	9.08	0.0190 +/- 0.0099	-0.2276	0.46	S Pacific
18	COOK14MV-22	-31.582	-177.258	27	9	0.75 +/- 0.08	6.23	0.0169 +/- 0.0089	0.8131	0.83	S Pacific
19	DRFT07RR-13	-37.270	-156.005	26	8	0.61 +/- 0.10	5.20	0.0125 +/- 0.0068	-0.8908	0.20	S Pacific
20	DRFT07RR-07	-33.236	-137.075	27	10	0.81 +/- 0.06	6.58	0.0149 +/- 0.0080	-0.5099	0.34	S Pacific
21	DRFT07RR-03	-29.203	-118.570	27	11	0.89 +/- 0.03	7.85	0.0210 +/- 0.0110	0.4319	0.73	S Pacific
22	AMT20-28	-29.943	-31.690	26	16	0.95 +/- 0.02	10.43	0.0225 +/- 0.0117	-0.0425	0.55	S Atlantic
23	AMT20-26	-23.838	-26.567	27	10	0.78 +/- 0.06	6.41	0.0179 +/- 0.0094	0.8403	0.84	S Atlantic
24	AMT20-24	-15.331	-21.841	25	11	0.87 +/- 0.04	7.70	0.0206 +/- 0.0108	1.4650	0.95	S Atlantic
25	AMT20-22	-6.057	-23.813	25	15	0.93 +/- 0.03	9.87	0.0183 +/- 0.0096	0.3090	0.68	S Atlantic
26	AMT20-21	-3.866	-25.018	25	14	0.89 +/- 0.05	9.16	0.0211 +/- 0.0110	0.2750	0.66	S Atlantic
27	MP3-34-03-00	3.591	-43.071	14	9	0.92 +/- 0.05	9.00	0.0234 +/- 0.0126	0.0288	0.56	N Atlantic
28	MP3-21-04-00	9.575	-45.304	27	15	0.94 +/- 0.03	9.98	0.0190 +/- 0.0100	-0.3055	0.43	N Atlantic
29	MP3-14-01-00	12.038	-55.262	27	11	0.79 +/- 0.07	7.01	0.0146 +/- 0.0078	-0.8446	0.21	N Atlantic
30	AMT20-16	13.455	-38.950	26	12	0.79 +/- 0.08	7.70	0.0172 +/- 0.0091	-0.3320	0.42	N Atlantic
31	AMT20-15	16.190	-35.806	26	12	0.75 +/- 0.09	7.44	0.0125 +/- 0.0068	-0.9649	0.17	N Atlantic
32	AMT20-13	21.212	-39.293	26	6	0.52 +/- 0.11	4.33	0.0079 +/- 0.0045	<b>-1.8981</b>	0.01	N Atlantic
33	AMT20-11	25.985	-38.783	27	7	0.64 +/- 0.10	5.14	0.0085 +/- 0.0048	<b>-1.6561</b>	0.03	N Atlantic
34	MP3-12-06-00	29.570	-45.026	26	13	0.90 +/- 0.04	8.59	0.0200 +/- 0.0105	0.0045	0.56	N Atlantic
35	MP3-08-03-00	29.427	-35.564	29	11	0.76 +/- 0.08	7.00	0.0118 +/- 0.0064	-0.9244	0.18	N Atlantic
36	AMT20-9	30.288	-34.181	31	7	0.57 +/- 0.10	4.69	0.0124 +/- 0.0067	-0.7867	0.23	N Atlantic
37	AMT20-7	34.203	-29.722	28	14	0.90 +/- 0.04	8.93	0.0169 +/- 0.0089	-0.7374	0.25	N Atlantic
38	MP3-02-06-00	29.096	-23.361	29	8	0.48 +/- 0.11	4.64	0.0079 +/- 0.0045	<b>-1.5364</b>	0.05	N Atlantic
39	AS1 Knorr	38.466	25.049	25	6	0.78 +/- 0.05	5.17	0.0150 +/- 0.0080	0.7949	0.82	Med Sea

Table 2.  $D_{24}$  (upper diagonal) and pairwise  $F_{57}$  (lower diagonal) between all collection sites in the global data set. Sample numbers correspond to those in Table 1. Significance level for  $F_{57}$  values are indicated by underlining ( $p \leq 0.000067$ , significant after Bonferroni correction) and bold ( $p \leq 0.05$ ). Within-gyre comparisons are italicized.

	1	2	3	4	5	6	7	8	9	10	11	12	13	14	15	16	17	18	19	20	21	22	23	24	25	26	27	28	29	30	31	32	33	34	35	36	37	38	39
1	*	<i>-0.017</i>	<i>0.026</i>	<i>0.013</i>	<i>-0.018</i>	<i>-0.003</i>	0.014	0.060	0.021	0.018	0.070	0.086	0.080	0.072	0.020	0.004	0.011	0.097	0.110	0.059	0.016	<i>-0.027</i>	0.053	0.015	<i>-0.019</i>	<i>-0.016</i>	<i>-0.027</i>	<i>-0.013</i>	0.064	0.052	0.077	0.162	0.121	<i>-0.006</i>	0.078	0.142	0.007	0.175	0.075
2	<i>0.003</i>	*	<i>0.052</i>	<i>0.056</i>	<i>0.020</i>	<i>0.042</i>	0.065	0.078	0.008	0.015	0.064	0.031	0.040	0.115	0.017	0.061	0.048	0.124	0.067	0.072	0.050	<i>-0.006</i>	0.092	0.050	<i>-0.006</i>	<i>-0.038</i>	<i>-0.041</i>	0.004	0.112	0.095	0.126	0.213	0.175	0.013	0.128	0.185	0.047	0.225	0.130
3	<i>0.053</i>	<i>0.090</i>	*	<i>-0.019</i>	<i>0.012</i>	<i>0.017</i>	0.096	0.147	0.107	0.107	0.156	0.138	0.160	0.157	0.110	0.086	0.094	0.160	0.165	0.127	0.089	0.005	<i>-0.002</i>	0.031	0.011	0.054	0.054	0.069	0.135	0.124	0.140	0.215	0.181	0.068	0.139	0.199	0.082	0.226	0.133
4	<i>0.036</i>	<i>0.089</i>	<i>0.001</i>	*	<i>-0.009</i>	<i>-0.009</i>	0.049	0.142	0.111	0.108	0.163	0.152	0.184	0.132	0.115	0.030	0.055	0.147	0.157	0.110	0.046	<i>-0.011</i>	0.004	0.013	0.005	0.065	0.053	0.057	0.115	0.102	0.117	0.190	0.155	0.068	0.119	0.185	0.073	0.210	0.125
5	<i>0.002</i>	<i>0.044</i>	<i>0.039</i>	<i>0.013</i>	*	<i>-0.025</i>	0.001	0.078	0.051	0.045	0.100	0.090	0.124	0.081	0.051	<i>-0.015</i>	0.011	0.069	0.136	0.043	0.006	<i>-0.028</i>	0.035	0.012	<i>-0.011</i>	0.016	<i>-0.006</i>	<i>-0.008</i>	0.040	0.034	0.047	0.123	0.087	0.004	0.053	0.107	0.006	0.136	0.059
6	<i>0.017</i>	<i>0.070</i>	<i>0.047</i>	<i>0.013</i>	<i>-0.005</i>	*	0.045	0.084	0.066	0.057	0.108	0.112	0.150	0.074	0.069	0.032	0.041	0.121	0.149	0.091	0.060	<i>-0.015</i>	0.030	0.019	0.005	0.041	0.026	0.032	0.099	0.099	0.112	0.197	0.152	0.049	0.114	0.177	0.053	0.210	0.108
7	<i>0.038</i>	<i>0.096</i>	<i>0.136</i>	<i>0.081</i>	<i>0.025</i>	<i>0.073</i>	*	0.125	0.103	0.095	0.154	0.146	0.179	0.113	0.102	<i>-0.009</i>	<i>-0.020</i>	<i>-0.004</i>	0.165	<i>-0.008</i>	<i>-0.024</i>	0.023	0.103	0.054	0.032	0.056	0.009	0.017	0.079	0.067	0.083	0.168	0.132	0.050	0.095	0.162	0.050	0.187	0.098
8	<i>0.094</i>	<i>0.126</i>	<i>0.208</i>	<i>0.193</i>	<i>0.115</i>	<i>0.126</i>	<i>0.173</i>	*	0.012	<i>-0.006</i>	<i>-0.019</i>	0.021	0.066	<i>-0.014</i>	<i>-0.009</i>	0.124	0.126	0.189	0.223	0.160	0.139	0.084	0.168	0.123	0.106	0.069	0.073	0.091	0.128	0.144	0.159	0.243	0.184	0.078	0.161	0.207	0.086	0.245	0.177
9	<i>0.048</i>	<i>0.038</i>	<i>0.159</i>	<i>0.154</i>	<i>0.082</i>	<i>0.101</i>	<i>0.143</i>	<i>0.048</i>	*	<i>-0.033</i>	<i>-0.009</i>	<i>-0.031</i>	<i>-0.017</i>	0.066	<i>-0.028</i>	0.100	0.102	0.169	0.199	0.133	0.116	0.042	0.142	0.087	0.069	<i>-0.007</i>	0.013	0.064	0.127	0.120	0.157	0.235	0.189	0.033	0.156	0.194	0.063	0.243	0.154
10	<i>0.042</i>	<i>0.044</i>	<i>0.155</i>	<i>0.148</i>	<i>0.074</i>	<i>0.090</i>	<i>0.132</i>	<i>0.019</i>	<i>-0.020</i>	*	<i>-0.009</i>	<i>-0.022</i>	<i>-0.002</i>	0.046	<i>-0.028</i>	0.097	0.098	0.162	0.196	0.128	0.108	0.043	0.140	0.090	0.067	0.001	0.018	0.058	0.118	0.116	0.148	0.230	0.182	0.035	0.148	0.191	0.060	0.237	0.151
11	<i>0.112</i>	<i>0.118</i>	<i>0.232</i>	<i>0.226</i>	<i>0.148</i>	<i>0.161</i>	<i>0.214</i>	<i>0.002</i>	<i>0.019</i>	<i>0.016</i>	*	<i>-0.007</i>	<i>0.019</i>	<i>0.024</i>	<i>-0.027</i>	0.150	0.151	0.211	0.240	0.179	0.164	0.099	0.187	0.138	0.123	0.051	0.072	0.107	0.150	0.158	0.185	0.264	0.208	0.081	0.186	0.222	0.101	0.266	0.201
12	<i>0.094</i>	<i>0.073</i>	<i>0.209</i>	<i>0.212</i>	<i>0.134</i>	<i>0.162</i>	<i>0.203</i>	<i>0.068</i>	<i>-0.019</i>	<i>-0.005</i>	<i>0.025</i>	*	<i>-0.025</i>	<i>0.091</i>	<i>-0.023</i>	0.144	0.145	0.206	0.230	0.167	0.157	0.075	0.178	0.124	0.107	0.014	0.043	0.102	0.161	0.153	0.192	0.265	0.221	0.062	0.192	0.222	0.096	0.272	0.195
13	<i>0.131</i>	<i>0.095</i>	<i>0.251</i>	<i>0.260</i>	<i>0.183</i>	<i>0.216</i>	<i>0.252</i>	<i>0.144</i>	<i>0.006</i>	<i>0.029</i>	<i>0.078</i>	<i>-0.009</i>	*	<i>0.147</i>	<i>0.001</i>	0.179	0.179	0.233	0.253	0.196	0.189	0.109	0.206	0.154	0.135	0.023	0.062	0.130	0.193	0.178	0.225	0.292	0.255	0.084	0.225	0.247	0.126	0.299	0.224
14	<i>0.104</i>	<i>0.159</i>	<i>0.211</i>	<i>0.178</i>	<i>0.115</i>	<i>0.112</i>	<i>0.156</i>	<i>0.004</i>	<i>0.114</i>	<i>0.086</i>	<i>0.066</i>	<i>0.156</i>	<i>0.234</i>	*	<i>0.034</i>	0.108	0.111	0.181	0.221	0.158	0.131	0.089	0.162	0.117	0.110	0.109	0.098	0.093	0.124	0.145	0.151	0.234	0.173	0.099	0.152	0.207	0.093	0.238	0.169
15	<i>0.048</i>	<i>0.049</i>	<i>0.164</i>	<i>0.160</i>	<i>0.087</i>	<i>0.104</i>	<i>0.143</i>	<i>0.017</i>	<i>-0.012</i>	<i>-0.013</i>	<i>-0.012</i>	<i>-0.004</i>	<i>0.039</i>	<i>0.072</i>	*	0.092	0.099	0.166	0.202	0.131	0.110	0.046	0.142	0.089	0.074	0.002	0.023	0.053	0.103	0.100	0.134	0.212	0.163	0.027	0.133	0.174	0.049	0.217	0.141
16	<i>0.025</i>	<i>0.089</i>	<i>0.122</i>	<i>0.058</i>	0.006	0.057	<i>0.016</i>	<i>0.167</i>	<i>0.136</i>	<i>0.130</i>	<i>0.203</i>	<i>0.194</i>	<i>0.244</i>	<i>0.147</i>	<i>0.135</i>	*	<i>0.006</i>	<i>0.095</i>	<i>0.169</i>	<i>0.071</i>	<i>-0.006</i>	0.009	0.097	0.041	0.037	0.062	0.038	0.004	0.022	0.007	0.020	0.079	0.051	0.013	0.025	0.078	0.004	0.097	0.046
17	<i>0.031</i>	<i>0.075</i>	<i>0.129</i>	<i>0.084</i>	<i>0.033</i>	<i>0.065</i>	<i>0.002</i>	<i>0.168</i>	<i>0.137</i>	<i>0.130</i>	<i>0.203</i>	<i>0.194</i>	<i>0.242</i>	<i>0.149</i>	<i>0.134</i>	<i>0.029</i>	*	<i>0.026</i>	<i>0.125</i>	<i>-0.009</i>	<i>-0.015</i>	0.016	0.099	0.051	0.017	0.049	0.011	0.021	0.101	0.091	0.103	0.196	0.157	0.058	0.117	0.185	0.063	0.215	0.112
18	<i>0.130</i>	<i>0.172</i>	<i>0.219</i>	<i>0.196</i>	<i>0.105</i>	<i>0.162</i>	<i>0.026</i>	<i>0.256</i>	<i>0.227</i>	<i>0.216</i>	<i>0.293</i>	<i>0.284</i>	<i>0.330</i>	<i>0.241</i>	<i>0.225</i>	<i>0.136</i>	<i>0.058</i>	*	<i>0.182</i>	<i>-0.023</i>	<i>0.032</i>	0.108	0.172	0.139	0.091	0.110	0.047	0.078	0.157	0.153	0.161	0.254	0.220	0.126	0.180	0.239	0.130	0.264	0.168
19	<i>0.161</i>	<i>0.127</i>	<i>0.251</i>	<i>0.230</i>	<i>0.191</i>	<i>0.211</i>	<i>0.234</i>	<i>0.318</i>	<i>0.284</i>	<i>0.274</i>	<i>0.353</i>	<i>0.339</i>	<i>0.385</i>	<i>0.303</i>	<i>0.286</i>	<i>0.231</i>	<i>0.185</i>	<i>0.277</i>	*	<i>0.119</i>	<i>0.120</i>	0.100	0.199	0.166	0.061	0.111	0.045	0.086	0.214	0.212	0.206	0.289	0.258	0.154	0.224	0.274	0.177	0.296	0.216
20	<i>0.087</i>	<i>0.110</i>	<i>0.176</i>	<i>0.150</i>	<i>0.072</i>	<i>0.125</i>	<i>0.019</i>	<i>0.218</i>	<i>0.182</i>	<i>0.174</i>	<i>0.250</i>	<i>0.235</i>	<i>0.281</i>	<i>0.209</i>	<i>0.181</i>	<i>0.105</i>	<i>0.013</i>	<i>-0.005</i>	<i>0.197</i>	*	<i>-0.002</i>	0.065	0.145	0.108	0.043	0.068	0.006	0.042	0.136	0.130	0.135	0.234	0.198	0.090	0.156	0.219	0.101	0.246	0.147
21	<i>0.038</i>	<i>0.080</i>	<i>0.127</i>	<i>0.076</i>	<i>0.029</i>	<i>0.085</i>	<i>-0.003</i>	<i>0.184</i>	<i>0.154</i>	<i>0.143</i>	<i>0.220</i>	<i>0.209</i>	<i>0.256</i>	<i>0.171</i>	<i>0.152</i>	<i>0.017</i>	<i>0.005</i>	<i>0.067</i>	<i>0.184</i>	<i>0.022</i>	*	0.028	0.111	0.068	0.019	0.057	0.010	0.008	0.063	0.051	0.055	0.138	0.106	0.039	0.071	0.138	0.040	0.156	0.086
22	<i>-0.008</i>	0.016	0.031	0.010	<i>-0.009</i>	0.006	0.049	<i>0.122</i>	<i>0.073</i>	<i>0.072</i>	<i>0.147</i>	<i>0.119</i>	<i>0.168</i>	<i>0.124</i>	<i>0.079</i>	<i>0.032</i>	<i>0.039</i>	<i>0.146</i>	<i>0.155</i>	<i>0.096</i>	<i>0.052</i>	*	<i>0.027</i>	<i>-0.001</i>	<i>-0.021</i>	<i>-0.002</i>	<i>-0.016</i>	<i>-0.004</i>	0.077	0.065	0.088	0.167	0.129	0.015	0.088	0.148	0.026	0.184	0.087
23	<i>0.083</i>	<i>0.135</i>	0.027	0.032	<i>0.065</i>	<i>0.062</i>	<i>0.145</i>	<i>0.231</i>	<i>0.196</i>	<i>0.189</i>	<i>0.264</i>	<i>0.251</i>	<i>0.297</i>	<i>0.218</i>	<i>0.197</i>	<i>0.134</i>	<i>0.135</i>	<i>0.233</i>	<i>0.286</i>	<i>0.196</i>	<i>0.151</i>	<i>0.057</i>	*	<i>-0.020</i>	<i>0.030</i>	<i>0.093</i>	<i>0.091</i>	<i>0.096</i>	0.159	0.152	0.169	0.241	0.206	0.111	0.169	0.227	0.117	0.255	0.163
24	<i>0.038</i>	<i>0.082</i>	<i>0.066</i>	<i>0.041</i>	<i>0.036</i>	<i>0.045</i>	<i>0.086</i>	<i>0.173</i>	<i>0.129</i>	<i>0.128</i>	<i>0.200</i>	<i>0.182</i>	<i>0.229</i>	<i>0.162</i>	<i>0.132</i>	<i>0.069</i>	<i>0.079</i>	<i>0.187</i>	<i>0.237</i>	<i>0.148</i>	<i>0.099</i>	<i>0.022</i>	<i>0.000</i>	*	<i>0.014</i>	<i>0.048</i>	<i>0.042</i>	<i>0.046</i>	0.108	0.095	0.119	0.188	0.154						

Table 3. Analysis of molecular variance (AMOVA) results comparing the northern and southern gyre populations in the Atlantic and Pacific Oceans ( $p < 0.00001$  for all fixation indices). The samples are grouped as in Fig. 5.

Ocean basin	Source of variation	df	Variance components	Percentage of variation	Fixation indices
Atlantic	among groups	1	1.174	21.16	$F_{CT}$ 0.211
	among populations	15	0.097	1.75	$F_{SC}$ 0.031
	within populations	427	4.277	77.10	$F_{IS}$ 0.235
Pacific	among groups	1	1.119	15.39	$F_{CT}$ 0.154
	among populations	13	0.395	5.43	$F_{SC}$ 0.064
	within populations	386	5.760	70.19	$F_{IS}$ 0.208

## Figures

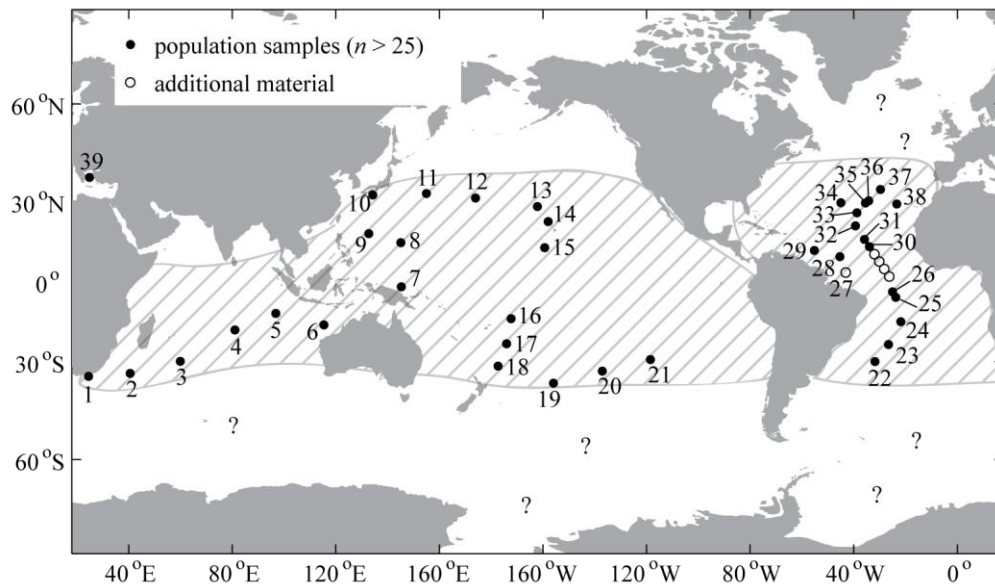


Figure 1. Collection sites for populations included in this study. Samples with  $n > 25$  individuals (closed symbols) are included in all analyses. Samples with  $n < 25$  individuals (open symbols) in the tropical Atlantic were included only in statistical parsimony analyses (Fig. 2). Collection sites are numbered as in Table 1. Hashed region indicates the approximate global biogeographic distribution of *Haloptilus longicornis*. A question mark indicates ocean regions in which *H. longicornis* has been reported to occur (Razouls et al. 2005-2012), but we consider these reports uncertain.

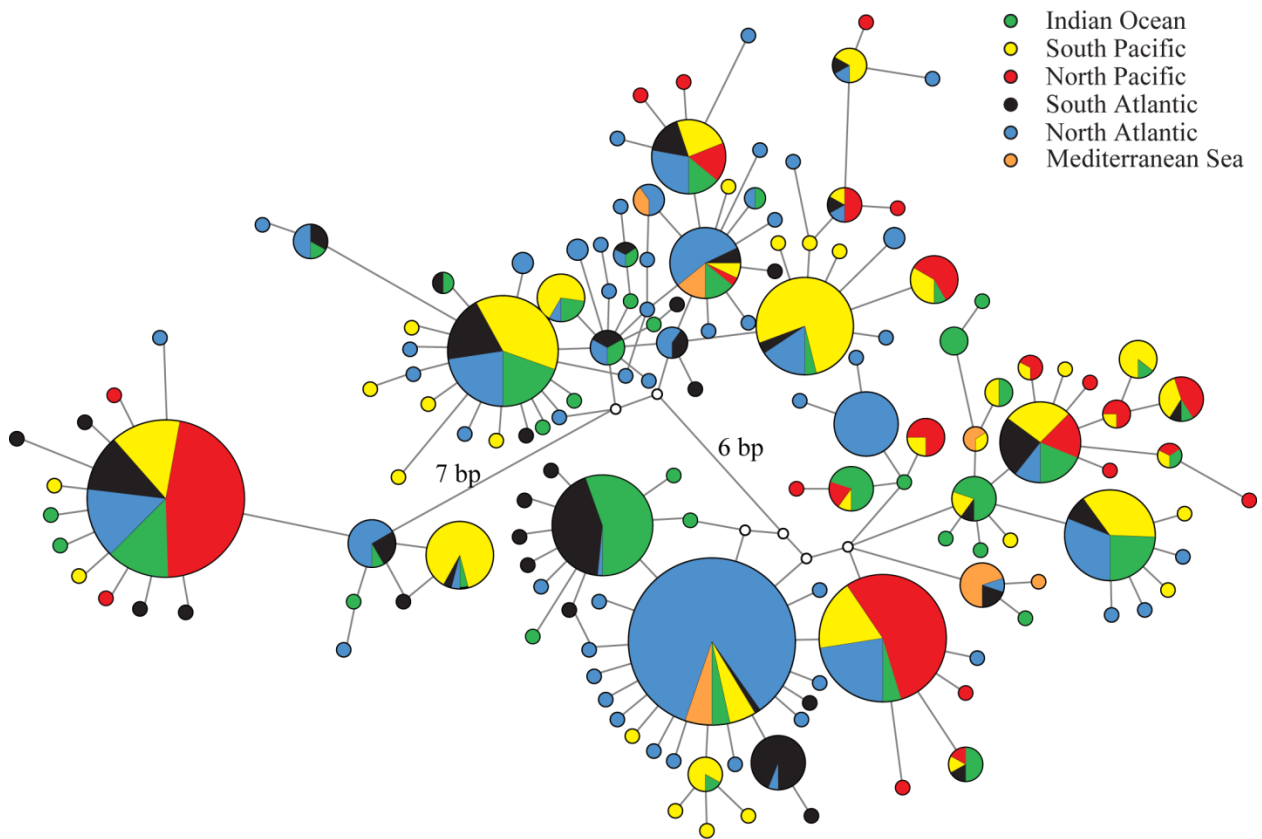


Figure 2. Statistical parsimony haplotype network for mtCOII haplotypes in *H. longicornis*. Each circle represents a unique haplotype (open circles represent unsampled haplotypes). The size of the circle is proportional to the number of specimens with that haplotype, and color indicates the geographic location from which the specimens were collected. The length of the edge is proportional to the number of mutations between haplotypes. There are two large genetic breaks, of 6 and 7 bp mutations (indicated on the figure), that separate haplotypes into three groups.

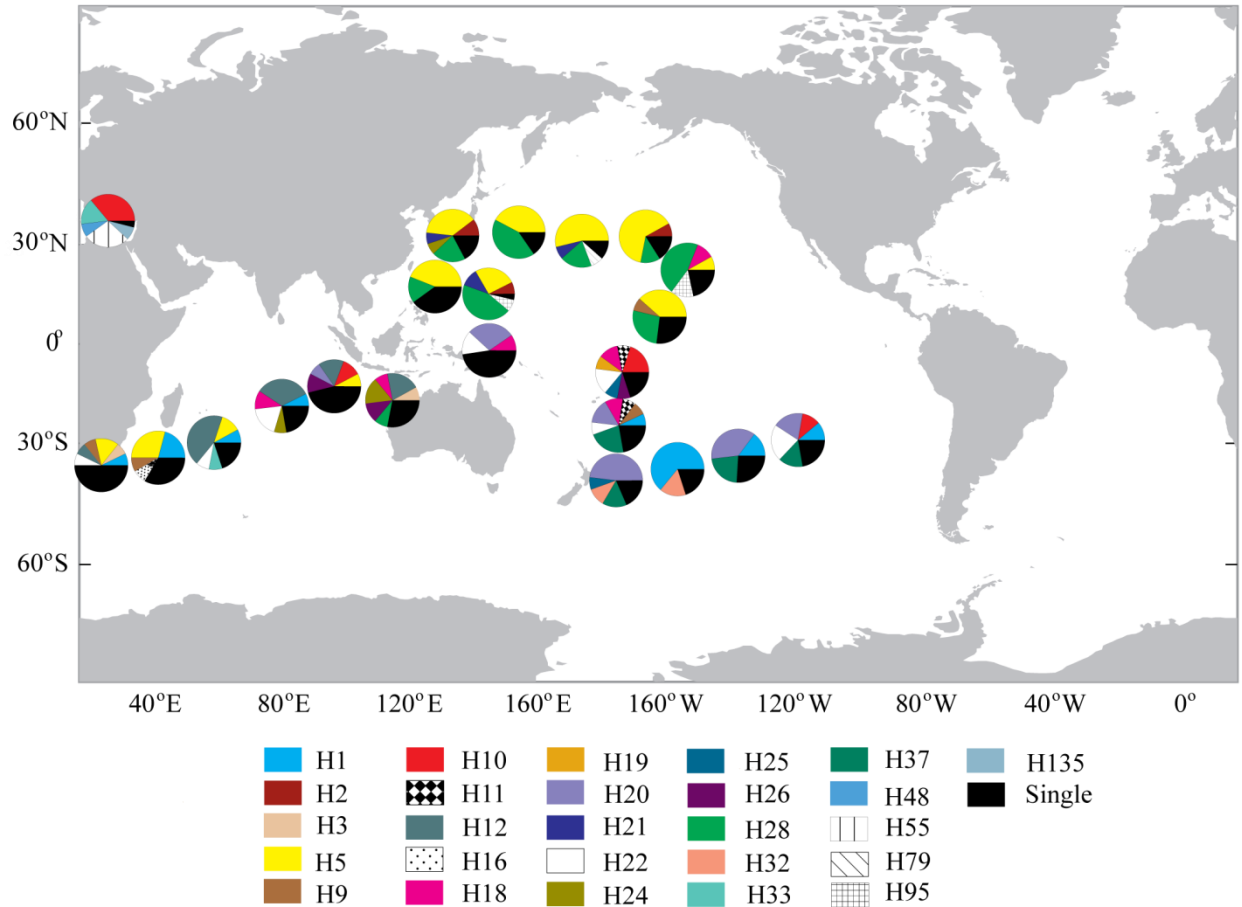


Figure 3. mtCOII haplotype frequencies in *Haloptilus longicornis*. Pies indicate the haplotype frequency found at each collection site from the global dataset, not including Atlantic samples (cruises MP3 and AMT20). Atlantic results are shown in Fig. 4. Haplotypes are labeled by pattern and color, according to the legend. Black includes all haplotypes that appear only once at any given site.

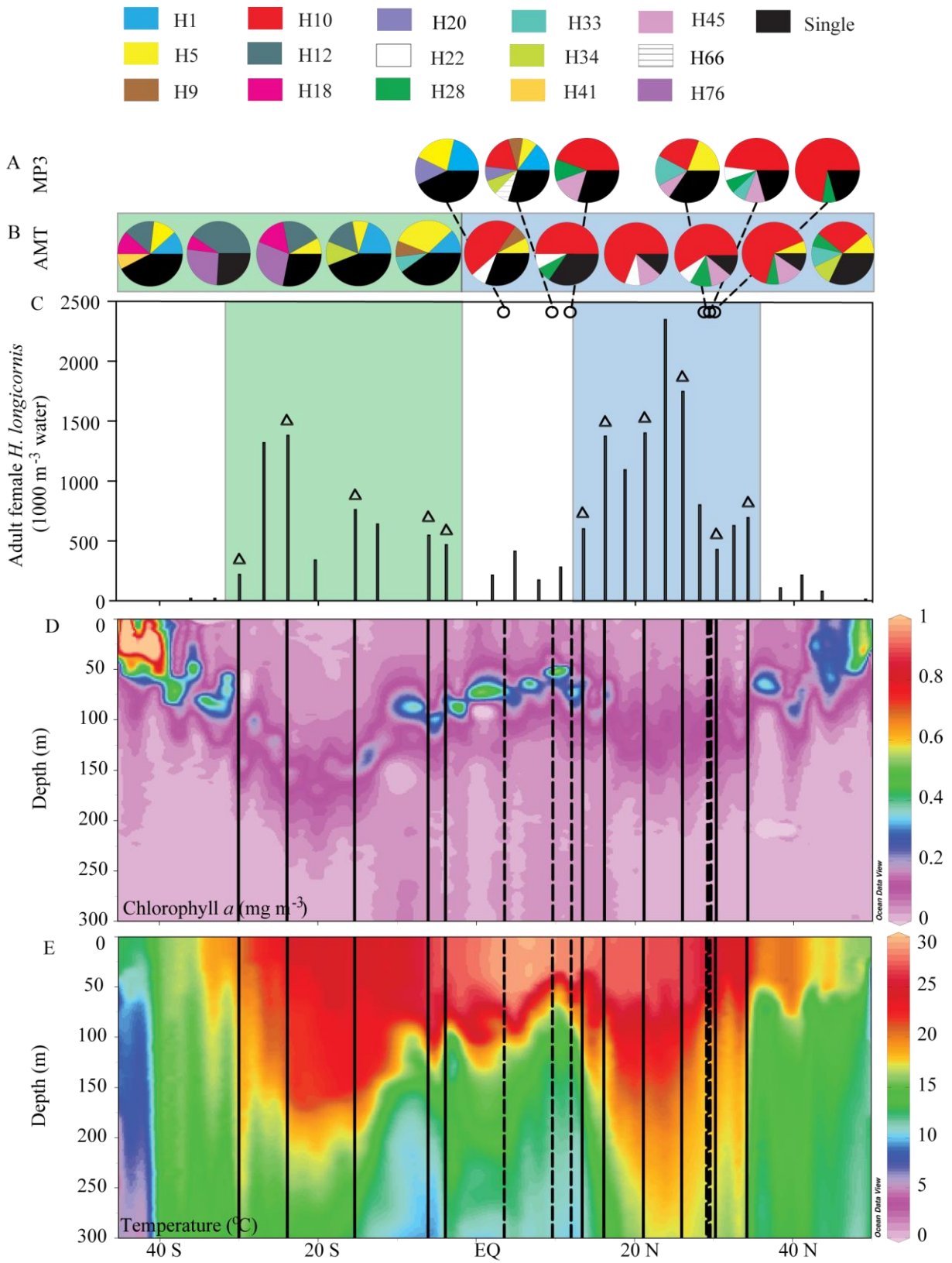


Figure 4. Environmental portrait of an open-ocean dispersal barrier in the Atlantic Ocean for *H. longicornis*. (A-B) Pies show mtCOII haplotype frequencies in population samples from (A) the MP3 cruise (Sites 27-29, 34-35, and 38) and (B) the AMT cruise (Sites 22-26, 30-33, and 36-37). Legend for haplotype color is shown at the top. (C) Abundance of *H. longicornis* adult females in the AMT samples, in individuals per 1000 m<sup>3</sup> of seawater filtered. Blue and green shaded boxes mark regions of suitable habitat in subtropical gyres of the northern and southern hemispheres, respectively. Triangles above the bars indicate the AMT collection sites for which we report haplotype frequencies in panel B. Small circles indicate the latitude at which samples from the MP3 cruise were collected (although not along this ocean transect). (D) Oceanographic transects of chlorophyll *a*, and (E) seawater temperature with respect to depth and latitude, from the 2010 Atlantic Meridional Transect cruise (AMT20). Solid lines indicate the collection sites for AMT samples. Dashed lines mark the latitude of collection for MP3 samples. Collection sites are numbered as in Table 1.

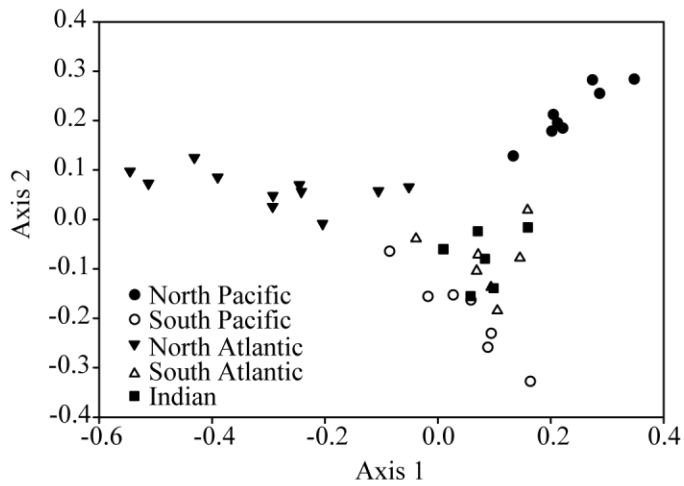


Figure 5. Principal coordinates analysis (PCoA) of all samples, based on pairwise  $F_{ST}$  values (Table 3). Symbols indicate the ocean region of collection (*see* Table 1 for details). Sites 27 and 28 are included with the South Atlantic samples.

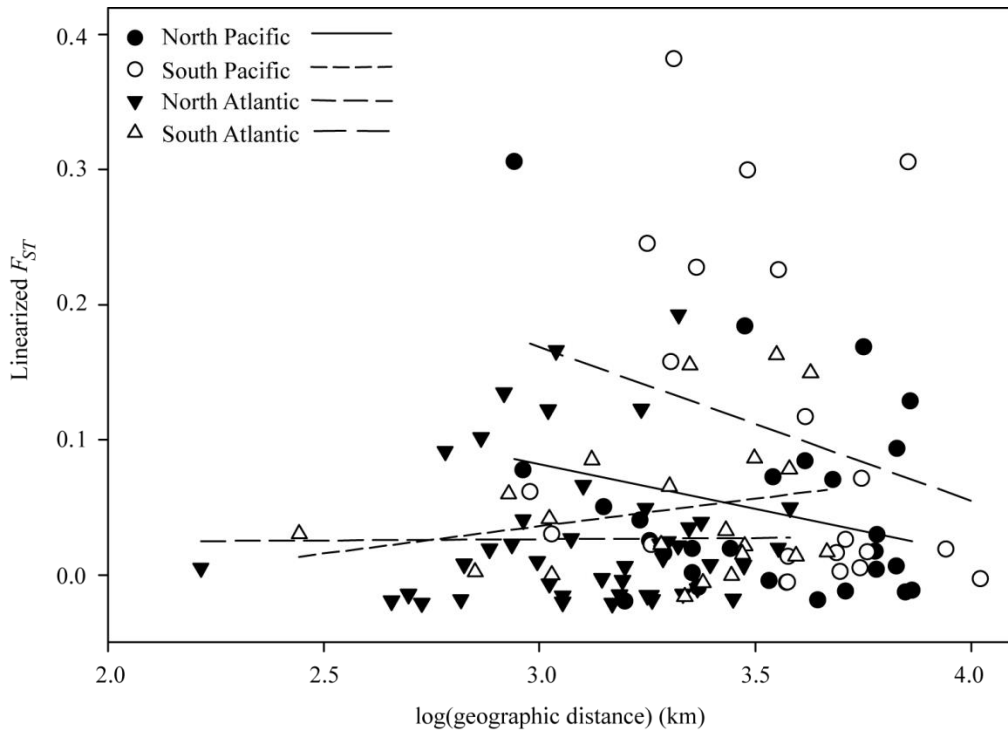


Figure 6. Isolation by distance was not observed within the four subtropical gyres of the Atlantic and Pacific Oceans ( $p \gg 0.05$ , Mantel tests). Non-significant linear regressions between linearized  $F_{ST}$  and  $\log(\text{geographic distance})$  for each subtropical gyre ( $p \gg 0.05$  for all), with symbol and regression line style for each gyre as shown in the legend. The tropical North Atlantic sites (Sites 27 and 28) are grouped with the South Atlantic populations.

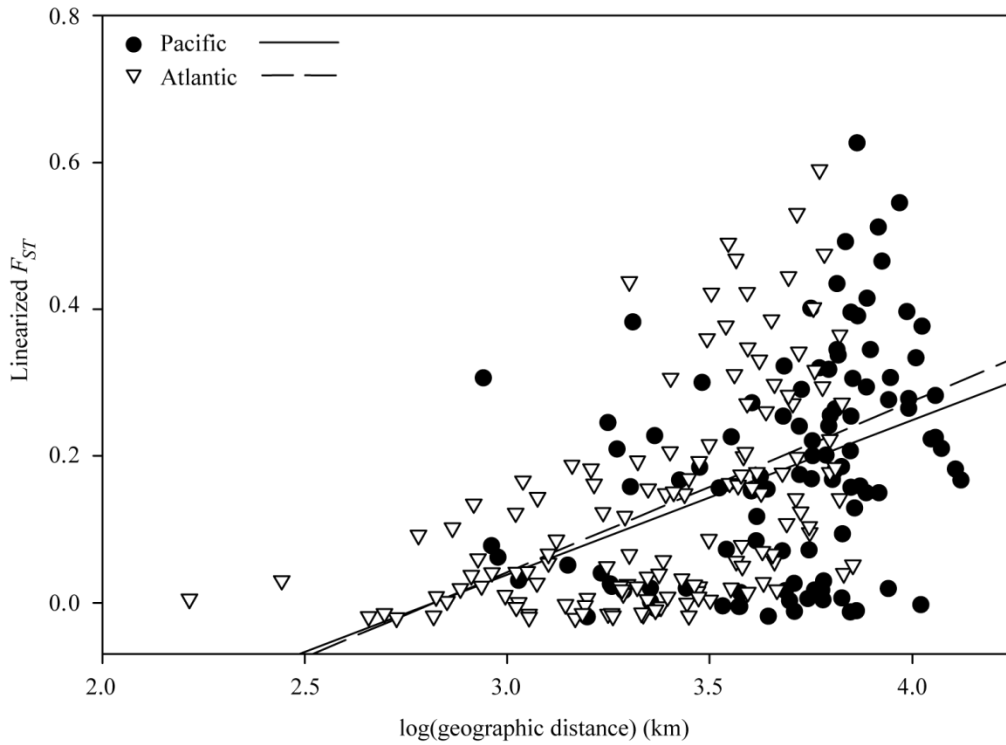


Figure 7. Isolation by distance at basin scales in the Atlantic and Pacific Oceans. Linear regression for the Atlantic Ocean comparisons (Linearized  $F_{ST} = -0.657 + (0.233 \times \text{Log}(\text{geographic distance}))$ ;  $R^2 = 0.266$ ;  $p < 0.001$ ) and the Pacific Ocean comparisons (Linearized  $F_{ST} = -0.593 + (0.210 \times \text{Log}(\text{geographic distance}))$ ;  $R^2 = 0.142$ ;  $p < 0.001$ ), with symbols and line styles in each ocean as shown in the legend. Both within and between gyre comparisons are included for each ocean.

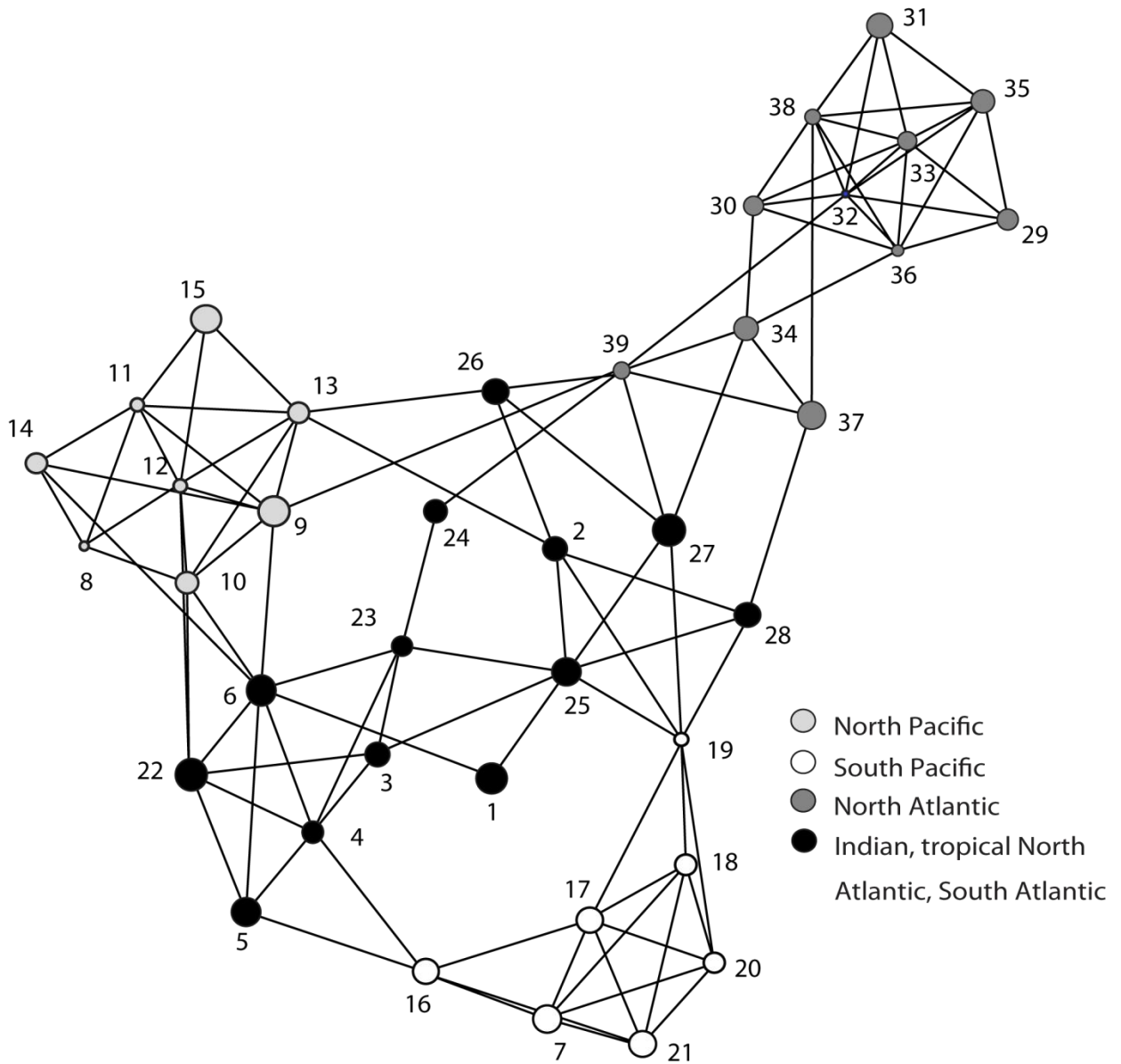


Figure S1. Population graph for all *H. longicornis* samples. Nodes (dots) represent populations: the shading indicates the geographic location of the collection site, and the size is proportional to the genetic diversity of the sample. Edges (lines) represent the covariance between populations. Population numbers as in Table 1.

## Chapter 2: A biophysical dispersal barrier for holoplankton in the equatorial Atlantic

### Abstract

In a previous study, genetic divergence was observed among subtropical gyre populations of the mesopelagic copepod, *Haloptilus longicornis*, in the Atlantic Ocean. In order to understand the mechanisms driving this genetic break, I investigated the dispersal routes and barriers in the equatorial Atlantic by simulating plankton dispersal at the 197 m depth layer of the Simple Ocean Data Assimilation (SODA) model using a particle-tracking scheme. Dispersal was simulated under three scenarios: 1) physical forcing alone, 2) physical forcing with elevated mortality of particles in the equatorial region, and 3) physical forcing with suppressed reproduction of particles in the equatorial region, in order to simulate poor quality habitat in this region. Particle dispersal simulations with physical forcing alone predicted that 26% of particles that originated within the southern subtropical gyre dispersed to the northern subtropical gyre over 30 years, which is an unrealistically high degree of connectivity given the empirical genetic divergence observed among the subtropical gyre populations in this copepod species. When biological processes were imposed in the equatorial region (higher mortality, lower reproduction), dispersal among gyres ceased due to the long equatorial residence times of particles in comparison to their expected longevity (minimum residence time was 6 months). These results indicate the presence of a biophysical dispersal barrier in the equatorial Atlantic that prevents contemporary dispersal among subtropical gyre populations for *H. longicornis*. I also investigated the possibility of using oceanographic dispersal probability instead of geographic distance to predict genetic distance among stations in the Atlantic Ocean, but found that dispersal probability was a poor predictor of genetic distance among sites.

## **Introduction**

Molecular techniques provide powerful tools for understanding the genetic structure of marine species and for inferring connectivity among populations. Because the degree of spatial genetic structure can be informative regarding migration among populations (e.g. open vs. closed populations; Cowen et al., 2000; Mora and Sale, 2002; Warner and Cowen, 2002; Cowen and Sponaugle, 2009), genetic structure is often studied to determine the best-fit migration model for understanding dispersal within a species (e.g. Pogson et al., 2001; Wirth and Bernatchez, 2001). Information on genetic structure within species also is used in designing marine reserves (e.g. Ferguson et al., 1995; Palumbi, 2003; Palsboll et al., 2007; Coleman et al., 2011) and to discover elusive dispersal barriers (e.g. Chapter 1; Keeney and Heist, 2006; Lessios and Robertson, 2006; Rocha et al., 2007). However, it is important to acknowledge the limitations of interpreting genetic structure in the context of connectivity (reviewed in Marko and Hart, 2011), because genetic patterns represent an integrated outcome of a number of processes, including genetic drift, mutation, selection, as well as migration, and it can be difficult to distinguish the relative importance of each (Wright, 1931; Slatkin, 1985). In addition, it can be difficult to differentiate between contemporary and historical processes acting on populations, in part because large marine populations take a long time to reach migration-drift equilibrium (Whitlock and McCauley, 1999). Biophysical models provide an alternative approach to investigating contemporary dispersal and connectivity among marine populations, and can provide either theoretical (e.g., Pringle and Wares, 2007) or spatially explicit (e.g., Baums et al., 2006) understanding of the mechanisms driving population genetic structure.

Our goal is to understand genetic connectivity among populations of a holoplanktonic organism at basin spatial scales in the Atlantic Ocean. Here I use a Lagrangian particle-tracking scheme and an ocean circulation model to better understand dispersal routes and barriers for holoplankton moving among subtropical gyres. This work builds on a prior genetic study of the mesopelagic copepod, *Haloptilus longicornis*, in which genetic divergence was observed among subtropical gyre populations in both the Atlantic and Pacific Oceans (Chapter 1). Within the Atlantic Ocean (the focus here), gyre populations were differentiated with pairwise  $F_{ST}$  values of -0.062 – 0.49 (mitochondrial cytochrome oxidase subunit II, mtCOII), and principal coordinates and analysis of molecular variance (AMOVA) results also suggested strong genetic structuring among gyres (AMOVA,  $F_{CT}=0.21$ ,  $p < 0.00001$ ). Genetic divergence was driven primarily by changes in haplotype frequency, although one private haplotype was observed in the North Atlantic. In addition, this genetic break across Atlantic equatorial waters coincided with a region of low abundance for *H. longicornis* (Fig. 1.4), and pilot experiments also indicated that reproduction likely does not occur in equatorial waters for this species (E. Goetze unpubl.). Taken together, these results indicate that the equatorial region is likely a region of lower quality habitat for this species, and may serve as a dispersal barrier for migrants traveling among subtropical gyre habitats. However, there are multiple possible mechanisms that could yield the genetic patterns observed, and biophysical modeling is one approach that can help distinguish between alternative mechanisms. Specifically, gene flow among gyre populations may be occurring contemporarily at low levels, or the high degree of haplotype sharing among gyres may reflect ancestral polymorphisms with no gene flow among populations in distinct gyres

(genetic drift ineffective in large populations; e.g., Whitlock and McCauley, 1999; Peijnenburg et al., 2005).

Biophysical modeling is a powerful approach that has not been previously applied to understand genetic connectivity in holoplanktonic marine species. Most published modeling studies on holoplankton investigate the abundance and distribution of plankton, often coupling an ocean circulation model with an individual based model (IBM) parameterized with life history characteristics of an organism (e.g. development, diapause, reproduction, feeding, and mortality; Bryant et al., 1998; Murphy et al., 1998; Batchelder et al., 2002; Speirs et al., 2005, 2006). Many, but not all, of these studies, were conducted over a smaller spatial domain than is of interest here, and they did not explicitly focus on resolving the underlying genetic structure of planktonic species. However, in benthic marine species with complex life cycles, biophysical modeling has been used to understand important biological and physical factors that influence planktonic larval dispersal, such as pelagic larval duration (PLD), larval behavior, ocean currents, and seasonal variation in current structure (Siegel et al., 2003; Hohenlohe, 2004; Paris et al., 2007; North et al., 2008; Trembl et al., 2008; Cowen and Sponaugle, 2009; Robins et al., 2013). Biophysical models can also be employed to investigate seasonal oceanographic dispersal barriers (Hohenlohe, 2004; Baums et al., 2006) and identify unlikely dispersal corridors (Dawson et al., 2005). Ocean circulation models also have been used to estimate Lagrangian dispersal distances of migrants (e.g. oceanographic distance), which were then substituted for Euclidean distances among stations within an isolation by distance (IBD) framework (White et al., 2010; Alberto et al., 2011). Since oceanographic distance takes into account circuitous dispersal pathways and oceanic barriers to dispersal, it has sometimes been found to be a better predictor of genetic distance

among marine populations than simple Euclidean distance (White et al., 2010; Alberto et al., 2011).

In this study, I use a Lagrangian particle tracking scheme and ocean circulation model to simulate dispersal of *H. longicornis* populations within the Atlantic basin. The goals of this study were to: (1) confirm whether the equatorial region likely acts as a dispersal barrier in this species, (2) investigate the mechanism of this barrier, and understand whether it occurs due to physical transport alone or whether biological processes must be involved, and (3) investigate whether oceanographic dispersal probability is a useful predictor of genetic distance among these holoplankton populations. I also was particularly interested in whether migration among subtropical gyre populations is asymmetric, with dominant dispersal occurring from the southern to northern gyre, as would be predicted by the flow field in the upper mesopelagic zone. Since prior estimates of species abundance and pilot studies on egg production in *H. longicornis* both suggested that the equatorial region of the Atlantic is poor quality habitat for *H. longicornis* (Chapter 1), I simulated dispersal and quantified connectivity among populations in the subtropical gyres under two schemes: 1) using physical oceanographic forcing alone, and 2) imposing increased mortality or decreased reproduction in the equatorial region to simulate poor quality habitat for this species. To address the third objective, I simulated dispersal among discrete sampling sites throughout the Atlantic basin, in order to compare oceanographic dispersal probability with genetic distance among these same sites (using genetic data from Chapter 1). These results show that the equatorial dispersal barrier must occur due to a biophysical mechanism, and that it likely impedes all contemporary migration among subtropical gyre populations in *H. longicornis*. I

also found that dispersal probability was a poor predictor of genetic distance among populations.

## Methods

### *Target species*

*Haloptilus longicornis* is a circumglobally-distributed copepod that lives between approximately 45 °N and 40 °S in the Atlantic, Pacific, and Indian Oceans (Saraladevi et al., 1979; Razouls et al., 2005-2012; Chapter 1). This species is abundant in the upper-mesopelagic zone, with primary depth habitat between ~100 – 400 m, and does not exhibit diel vertical migration (McGowan and Walker, 1979; Ambler and Miller, 1987). Animals are ~1.7 – 2.6 mm in length (adult females), and are thought to be omnivores and detritus feeders (Hopkins, 1985). The life history of *H. longicornis* is not well known, but the longevity of this organism is likely on the order of 30 days (or less), as observed in other planktonic marine calanoids (e.g., Peterson, 1985; Kimmerer and McKinnon, 1987).

### *Study region – Atlantic basin*

The most likely mechanism for migration of *H. longicornis* among subtropical gyre populations is via the North Brazil Undercurrent (NBUC) and North Brazil Current (NBC; Fig. 1). These currents may transport animals from the southern to the northern subtropical gyre because they traverse the equatorial region near the Brazilian coastline. The North Brazil Undercurrent (NBUC) begins south of 10 °S, and is fed from southern hemisphere waters. At 10 °S the maximum velocity for this current is ~80 cms<sup>-1</sup> at a depth of ~250 m. As it travels northward, the core shoals to 150 – 200 m at 5 °S and eventually feeds into the surface-intensified NBC near the equator. From January to June the NBC continues to travel northward, forming the Guiana Current along the western boundary of the tropical Atlantic, transporting ~11 Sv of water northward between ~100 – 300 m (Schott et al., 1998).

However, from July to December, the NBC retroflects back into the North Equatorial Counter Current (NECC) and Equatorial Undercurrent (EUC; Metcalf and Stalcup, 1967; Johns et al., 1990; Richardson et al., 1994). During this period, stochastic eddies form, typically at  $\sim 7^\circ\text{N}$  and continue to travel northwestward toward the Caribbean (Johns et al., 1990; Richardson et al., 1994). It is estimated that these eddies provide substantial transport to the northern hemisphere, on the order of  $\sim 3\text{ Sv}$ , during the period of NBC retroflection (Richardson et al., 1994). Thus, dispersal of particles from the southern to northern hemispheres would be fastest from January to June, but could also occur via stochastic eddies from July to December, if particles were not entrained in the zonal equatorial currents.

At 197 m depth, there are several zonal currents in the equatorial region that may impede plankton dispersal among subtropical gyres (Fig. 1). For example, the Equatorial Undercurrent (EUC), which is located between  $\sim 2.5^\circ\text{N}$  and  $2.5^\circ\text{S}$  and transports  $\sim 17.5 \pm 4.4\text{ Sv}$  (mean  $\pm$  s.d.) of water eastward between  $\sim 100\text{ m}$  and  $300\text{ m}$  depths, is primarily fed by the retroflection of the North Brazil Current (Reid, 1964; Schott et al., 1998). Thus, if particles traveling in the NBC get retroflected to the EUC, they will be advected zonally toward the coast of Africa, and the amount of time they spend in the poor quality equatorial habitat will increase. However, if particles in the eastern Atlantic become entrained in the westward-flowing Southern Equatorial Current (SEC), located between  $\sim 4 - 25^\circ\text{S}$ , or the Northern Equatorial Current (NEC), located between  $\sim 7 - 20^\circ\text{N}$ , these particles will be advected toward the western side of the equatorial region and may join the NBUC or NBC (Schott et al., 1998; 2002).

*Ocean circulation model and particle-tracking scheme*

Dispersal of *H. longicornis* was simulated using the Simple Ocean Data Assimilation (SODA) model (SODA version 2.2.4; Carton et al., 2000a, b). This is a 3-dimensional hindcast model based on the Parallel Ocean Programs (POP) model. SODA is forced with Twentieth Century Reanalysis version 2 (20CRv2) ensemble mean winds and corrected with oceanographic data (WOD09, COADS 2.5 SST). This model is global in scope, with an average horizontal resolution of 0.5 x 0.5 degrees, and has 40 vertical levels. For this study, I used only the 197 m depth layer, which corresponds to the core habitat for *H. longicornis*. Monthly velocities are available for this model for the years 1871-2008. I used a simple 4<sup>th</sup> order Runge-Kutta particle-tracking scheme to integrate particle movement throughout the Atlantic Ocean basin. As described more fully below, particles were released once at the beginning of the experiment every one degree over the entire width of the ocean basin between 45 °N and 40 °S, which represent the distributional limits for this species. Due to the large study domain, the horizontal resolution of the model and the relatively slow ocean velocities, particle velocities were updated every five days according to the ocean velocities at their coordinate location. Latitude and longitude coordinates were recorded every 5 days for each particle unless one of the following events occurred: 1) a particle struck land, and its velocity went to zero, or 2) a particle traveled poleward across the 45 °N or 40 °S boundary. In either of these cases, the particle was considered no longer viable and its path was not subsequently tracked. Within the context of this study, each particle represents an adiabatic parcel of water that contains an assemblage of copepods that are approximately in steady-state with respect to reproduction and mortality, rather than an individual plankter.

#### *Simulations – Sensitivity analyses*

Sensitivity analyses were run in order to determine whether dispersal patterns were influenced by the month and year in which simulations were initialized. Particle dispersal was simulated using velocity climatologies averaged two ways: 1) for each month over the entire 110 years of the model, and 2) for each year of the model. Results from these simulations were compared to results from simulations in which particles were dispersed in different months and years using monthly SODA velocities. All simulations were run for 100 years and were analyzed by calculating the degree of connectivity among Atlantic regions (*see* ‘Connectivity analyses’ below). These analyses revealed that dispersal patterns were sensitive to the month and year in which particles were dispersed (results not shown). Additionally, I found that it took approximately 30 years for full connectivity to develop among regions in the Atlantic basin (*see* Results). Therefore, in order to account for inter-seasonal and interannual variability in dispersal, a total of 100 simulations were initialized at randomly selected months and years (between 1875-1957), and each simulation was integrated for 30 years.

#### *Simulations – Particle dispersal*

For the first suite of experiments, I investigated dispersal among subtropical gyre populations of *H. longicornis* under two conditions: (1) with physical oceanographic forcing alone, and (2) including simple biological processes in the equatorial region, which I expect to be a region of poor quality habitat for this species (Chapter 1). Particles were initialized and advected in the 197 m depth layer of the model, given the preferred habitat depth of the species. Six particles were initialized every one degree over the entire width of the basin between 45 °N and 40 °S, for a total of ~31,500 particles. Particles were advected for 30

years and coordinate positions were recorded every 5 days, unless the particle was no longer viable (*see* above). By the end of the 30 year simulations, an average of 49.5% of particles were no longer viable (~15,609 particles). Results from this initial experiment were used to address the first hypothesis: with physical forcing alone, I hypothesized that dispersal among subtropical gyres would be asymmetric with dominant dispersal occurring from south to north.

In a second suite of experiments, I simulated dispersal among gyres with increased mortality or decreased reproduction within the equatorial region (Regions 8-11; Fig. 2; *see* below). Therefore, I used two approaches in order to simulate dispersal across this region (Fig. 3). In the first approach, I used an exponential decay function ( $P_t = P_o e^{-kt}$ ) to simulate mortality, where  $P_t$  is the population size at time  $t$ ,  $P_o$  is the initial population size, and  $k$  is the instantaneous mortality rate. With a  $k = 0.0126 \text{ day}^{-1}$ , I decreased the equatorial population size of *H. longicornis* by ~6% every five days such that the population of particles declined to 1% of its initial size after one year. This instantaneous mortality rate ( $k = 0.0126 \text{ day}^{-1}$ ) is conservative compared to stage-specific mortality estimates reported for planktonic copepods in the field (e.g.  $k = 0-2.17 \text{ day}^{-1}$ , *Clausocalanus furcatus*, Bi et al., 2011;  $k = 0-0.36 \text{ day}^{-1}$ , *Calanus finmarchicus*, Ohman et al., 2004;  $k = 0.14 \text{ day}^{-1}$ , broadcast spawners, Hirst and Kiorboe, 2002). Since reproduction often ceases under poor environmental conditions and when animals are expatriated out of their core pelagic habitat (e.g. Hirst and Bunker, 2003), I simulated a lack of reproduction in *H. longicornis* in equatorial waters by terminating particles that remained in the equatorial region for >30 consecutive days (i.e. the estimated generation time of this species). Results from these simulations were used to

address my second question: does the simulation of poor quality habitat in the equatorial region result in a biophysical barrier to dispersal among subtropical gyre populations?

### *Connectivity Analyses*

In order to quantify particle dispersal among ocean regions in the Atlantic, I calculated the dispersal probability among 15 biogeographic provinces by recording the proportion of particles originating in one region that dispersed to another region. The 15 biogeographic provinces within the study domain were characterized by distinct ecosystem structure and function, which were defined using plankton community composition, environmental, and physical oceanographic data (as defined by Longhurst, 2007; Fig. 2). The North Atlantic Subtropical (West) Gyral Province (NAST (W); Region 2) and the North Atlantic Tropical Gyral Province (NATR; Region 6) were combined to capture the northern subtropical gyre. The South Atlantic Gyral Province (SATL; Region 13) includes the entire southern subtropical gyre. Both subtropical gyres are thought to be preferred habitat for this species, while the equatorial region is likely poor quality habitat (*see* Chapter 1). The equatorial region was defined by four regions located between 12 °N and 10 – 15 °S: the Guianas Coastal Province (GUIA), Western Tropical Atlantic Province (WTRA), Eastern Tropical Atlantic Province (ETRA), and Guinea Current Coastal Province (GUIN; Regions 8-11, respectively).

Dispersal probability matrices were generated after 1, 5, 15, 25, and 30 years of particle simulations, in order to examine how dispersal patterns change over time. Particular attention was paid to dispersal among subtropical gyre populations, and I calculated the number of unique particles originating in one subtropical gyre that successfully dispersed to

the opposite gyre over the course of 30 years (Regions 2 and 6 = northern gyre, Region 13 = southern gyre; Fig. 2). In order to understand the time-scale to traverse the equatorial region, I calculated the residence time for particles in the equatorial region. When I imposed poor quality habitat in the equatorial region, I also recorded the times and locations at which particles were terminated within the equatorial region, and calculated the distance each particle had traveled within the equatorial region before it died.

#### *Estimating the number of migrants*

Using the mtDNA genetic data (Chapter 1) and the particle dispersal model results (this study), I estimated the number of particles predicted to disperse among subtropical gyre populations when physical forcing alone was used to simulate particle dispersal. Using effective population size ( $N_e$ ) as a conservative estimate of census size ( $N$ ), I estimated  $N_e$  for the northern and the southern subtropical gyre populations separately, using  $\Theta = 2N_e\mu$ , where  $\Theta$  is a measure of population diversity within a species and  $\mu$  is the per-generation mutation rate. One way to estimate  $\Theta$  is by calculating the number of segregating sites within a population ( $\Theta_s$ ), which I did from the genetic data from Chapter 1 (Arlequin version 3.5; Tajima, 1996; Excoffier and Lischer, 2010), and I obtained an estimate for the mitochondrial genome mutation rate from the literature (Knowlton and Weigt, 1998; Schubart et al., 1998).

#### *Isolation by oceanographic distance (IBOD)*

In a third suite of experiments, I investigated the probability of particle dispersal between sampling sites in the Atlantic when biological processes were simulated in the equatorial region, and compared this to genetic distance among populations of *H. longicornis*

collected at these same sites (Table 1). These simulations were identical to those in the first experiment, with the exception that 500 particles were released randomly within a 1 degree radius of all 13 Atlantic sampling stations (Table 1; Fig. 4). Dispersal probability among stations was averaged for all 100 simulations, then maximum dispersal probability was calculated for each pair of Atlantic stations, which were defined as  $2^{\circ} \times 2^{\circ}$  boxes centered at each station. For each pair of stations, Linearized  $F_{ST}$  (Table 2; data from Chapter 1; Rousset, 1997) was regressed on maximum dispersal probability among stations (ordinary least-squares linear regression; Breusch-Pagan test for heteroscedasticity). These results were compared to regressions of Linearized  $F_{ST}$  on Euclidean geographic distance (from Chapter 1; mtDNA group 1 haplotypes only included), in order to determine which distance metric was a better predictor of genetic distance. I also tested for IBOD by calculating the covariance of the genetic distance (Linearized  $F_{ST}$ ) and dispersal probability matrices for the within-gyre comparisons (Mantel test; Arlequin version 3.5).

## Results

### *Dispersal among gyres: Physical forcing*

Dispersal among regions within the Atlantic Ocean took ~ 30 years to develop fully (Fig. 5). During the first year, local retention was high, but connectivity also began to develop among adjacent regions, with moderate connectivity from Guianas to the Western Tropical Atlantic (Region 8 to 9), from the Benguela Current to the Southern Tropical Atlantic (Region 14 to 13), and from the Canary Current to the Northern Tropical Atlantic (Regions 7 to 6). After the first five years, local retention decreased while dispersal strengthened among non-adjacent regions (e.g. from the North Atlantic Tropical Gyre to the Gulf Stream Current (Region 6 to 1) and from the Benguela Current to the Guianas (Region 14 to 8)), and particles successfully dispersed from the southern to the northern subtropical gyre (Region 13 to 6). From 5 – 25 years after the simulations began, connectivity continued to strengthen among distant regions, with dispersal occurring primarily from southern (Regions 12-14) to northern regions (Regions 1, 5, 6). Dispersal probability among regions changed by less than 1% between years 25 and 30, suggesting that connections among distant regions were well established by the end of 30 years. Overall, the Guianas (Region 8) and the Western Tropical Atlantic (Region 9), both located in the equatorial region, had high connectivity with both the northern and southern hemisphere regions though they dispersed more particles to the northern hemisphere and received more particles from the southern hemisphere (Fig. 5).

After a 30 year simulation with physical forcing alone, contemporary dispersal among subtropical gyres was highly asymmetric, with dominant dispersal occurring from south to north (Fig. 6). Over the course of 30 years, 26% of particles originating in the southern

subtropical gyre dispersed to the northern subtropical gyre (Fig. 6B). The highest rate of arrival of particles occurred at 78 months (or ~6.5 years) after the simulation began, with ~0.22% of particles arriving per month. In contrast, only ~0.42% of particles originating in the northern subtropical gyre dispersed to the southern subtropical gyre over the 30 years, and the maximum rate of arrival occurred at 227 months (or ~18.9 years) with ~0.0058% of particles arriving per month (Figs. 6A, B).

Residence time in the equatorial region was shorter for particles dispersing from south to north than vice versa (Fig. 7A, B). Particles originating in the southern subtropical gyre that dispersed to the northern subtropical gyre had a minimum equatorial residence time of ~6 months and a mean residence time of ~5 years (Fig. 7A). However, particles originating in the northern subtropical gyre that successfully dispersed to the southern subtropical gyre spent a minimum of 16 months in the equatorial region and had a mean residence time of ~11 years (Fig. 7B). Most particles, migrating in both directions, entered the equatorial region near the western boundary, in Region 8. Particles with the shortest residence times in the equatorial region, and consequently the fastest dispersal rates among subtropical gyres, traversed the equatorial region via the North Brazil Current (NBC; Regions 8 and 9; Fig. 8). However, when particles were entrained in equatorial currents and were advected zonally toward the eastern boundary, through Regions 8, 9, 10, and 11, their equatorial residence times increased substantially (data not shown).

#### *Dispersal among gyres: Biophysical oceanography*

When simulations included biological processes, in order to simulate poor quality habitat for this species, the equatorial region served as a hard barrier to dispersal among

subtropical gyre habitats. Unsuitable habitat was simulated in the equatorial region by imposing elevated mortality or an absence of reproduction. All particles ‘died’ in these model runs, with the exception that in six of the higher mortality simulations (of 100 total simulations), one particle successfully dispersed from the southern to the northern gyre. Overall, particles were terminated more quickly under the decreased reproduction scenario than under the increased mortality scheme, which caused the death locations of particles to be closer to the boundary of the equatorial region (Fig. 9). In both the decreased reproduction and increased mortality simulations, mean dispersal distance in the equatorial region was farther for particles traveling from the southern to the northern subtropical gyre (decreased reproduction:  $689 \pm 315$  km, mean  $\pm$  std.; increased mortality:  $998 \pm 926$  km) than for particles dispersing from the northern to the southern subtropical gyre (decreased reproduction:  $129 \pm 65.6$  km; increased mortality:  $254 \pm 361$  km).

#### *Estimating the number of migrants*

Using the genetic data from Chapter 1, I estimated  $\Theta_{South}$  to be 4.12 and  $\Theta_{North}$  as 3.32. An approximate mutation rate estimate for the mitochondrial genome for crustaceans is ~1.5% per site per million years (Knowlton and Weigt, 1998; Schubart et al., 1998) and the longevity of planktonic calanoid copepods is on the order of 1 month (e.g., Peterson, 1985; Kimmerer and McKinnon, 1987), which results in a  $\mu$  of  $\sim 1.25 \times 10^{-9}$  substitutions per site per generation. Applying  $\Theta = 2N_e\mu$ , and solving for  $N_e$ , I estimate  $N_{e\ South}$  to be  $\sim 1.65 \times 10^9$  copepods, and  $N_{e\ North}$  to be  $\sim 1.33 \times 10^9$  copepods. At the end of the 30 year simulations, the model with physical oceanographic forcing alone predicted that ~0.05% of particles originating in the southern gyre dispersed to the northern gyre every generation, and

~0.001% of particles originating in the northern gyre dispersed to the southern gyre every generation. Therefore, dispersal simulations with physical forcing alone predicted that a minimum of ~824,000 particles disperse from the southern to the northern gyre and ~13,300 particles disperse from the northern to the southern gyre every generation. Since every particle represents an assemblage of copepods and because  $N_e \leq N$ , then I estimate that at least 824,000 copepods disperse from the southern to the northern gyre and at least 13,300 copepods disperse from the northern to the southern gyre every generation.

#### *Isolation by Oceanographic Distance – Comparing genetic and oceanographic distance*

With physical oceanographic forcing alone, dispersal occurred both among stations located within the same gyre and from the southern to the northern gyre stations (Fig. 10A). Over the course of the 30 year simulations, maximum connectivity per month among stations within the southern gyre ranged from 0.36 – 7.5%, while connectivity within the northern gyre ranged from 0.44 – 62%. For stations located in opposite gyres, connectivity ranged from 0 – 22%. However, when biological processes were incorporated in the equatorial region, connectivity decreased substantially both within and among gyres. Connectivity in the southern gyre ranged from 0.004 – 4.9%, while connectivity in the northern gyre ranged from 0.013 – 51%. Connectivity among stations in opposite gyres halted completely (Fig. 10B; min = 0, max = 0).

Using the maximum dispersal probability among stations when biological processes were simulated in the equatorial region, I found no significant relationship between genetic distance and maximum dispersal probability for within-gyre station comparisons (Fig. 11, linear regression,  $p > 0.05$ ; Breusch-Pagan test for heteroscedasticity,  $p > 0.05$ ; Mantel test,

$p \gg 0.05$  for both gyres), and there was no dispersal among stations in opposite gyres. Thus, dispersal probability between stations within gyres has effectively no explanatory power for linearized genetic distance among those same sites.

## Discussion

In meroplankton, dispersal barriers are often driven by the finite pelagic larval duration (PLD), which, in combination with the physical flow field, can prevent dispersal over long distances or across complex oceanographic features where there is no suitable settlement habitat (e.g. Gilg and Hilbish, 2003; Kool et al., 2010, 2011). Reproductive season, in combination with seasonal variability in ocean current structure, also has been reported to create effective barriers to dispersal for meroplankton (Hohenlohe, 2004; Baums et al., 2006). Since holoplankton spend their entire lives in the pelagic environment, do not require settlement habitat, and are able to reproduce continuously in suitable environmental conditions (e.g. Breteler, 1980), the mechanisms underlying dispersal barriers in many meroplanktonic species are unlikely to apply to holoplankton. This is the first study to integrate biophysical modeling (Chapter 2) and empirical genetic data (Chapter 1) to understand genetic connectivity in a holoplanktonic species, and I use this approach to clarify the mechanisms underlying an observed genetic break across equatorial waters in the common mesopelagic copepod *Haloptilus longicornis*. My results suggest that the equatorial dispersal barrier observed in this species must be biophysical in nature. Because I used a general ocean circulation model (GCM) coupled with a particle tracking scheme that was parameterized by only a few biological characteristics, such as habitat depth, generation time, and latitudinal boundaries for *H. longicornis*, these results are generally applicable to other species of the holoplankton community with similar biological niches.

Simulations with physical oceanographic forcing alone predicted unrealistically high rates of dispersal among subtropical gyre populations. Over the course of 30 years, the model predicted high levels of dispersal among gyres (26% of particles migrate, cumulative),

with dominant dispersal occurring from the southern to the northern subtropical gyre. Dispersal was approximately two orders of magnitude lower from the northern to the southern gyre (0.42% of particles, cumulative), indicating highly asymmetric dispersal, as was initially expected given the flow structure in the upper mesopelagic zone of the Atlantic basin. However, I infer that these dispersal rates are unrealistically high given the level of genetic differentiation observed among subtropical gyre populations of *H. longicornis* (Chapter 1). It is expected that, on average, one migrant per generation should be sufficient to prevent genetic differentiation among populations (one-migrant-per-generation rule; Spieth, 1974; Slatkin, 1985, 1987), although subsequent work has shown that up to 10-20 migrants per generation may be required to truly homogenize sub-populations (Mills and Allendorf, 1996; Vucetich and Waite, 2000). Chapter 1 reported significantly different haplotype frequencies in the northern and southern subtropical gyre populations of *H. longicornis*, as well as the presence of a private haplotype in the northern subtropical gyre population. Thus, I would expect very low levels of contemporary migration among these gyre populations (< 10 migrants per generation). The conservative migration estimates reported here, of 824,000 and 13,300 copepods dispersing from the southern to the northern gyre and vice versa, respectively, are still several orders of magnitude higher than the one-migrant-per-generation rule (Spieth, 1974; Mills and Allendorf, 1996). If migration among gyres were actually occurring at these rates, no differences in allele frequencies would be observed among subtropical gyre populations, and I would expect to find no private alleles in either gyre population. Therefore, I infer that physical oceanographic processes alone are insufficient to create a dispersal barrier for copepod migrants moving among subtropical gyres, even in the relatively-quiescent, mesopelagic portions of the water column.

When conservative biological constraints were imposed in the equatorial region, dispersal among gyres ceased, suggesting the presence of a biophysical dispersal barrier in the equatorial Atlantic that prevents migrants from dispersing among subtropical gyre habitats. The fastest migrants, dispersing from the southern to the northern gyre, traversed the equatorial region via the North Brazil Current (NBC), but the minimum equatorial residence time was still 6 months. I estimate the shortest dispersal distance between subtropical gyres via the NBC at ~4200 km, which implies an average dispersal velocity of ~27 cm/s for the fastest migrants traveling along this route. This dispersal rate estimate is within the range of velocities reported for the NBC below ~150 m depth (~20-40 cm s<sup>-1</sup>; Flagg et al., 1986). With an expected copepod lifespan of approximately 1 month (Peterson, 1985; Kimmerer and McKinnon, 1987), these long equatorial residence times suggest that successful dispersal among gyres would require multiple generations to survive and reproduce in this region. This is unlikely because high mortality and/or low reproduction are expected throughout the equatorial region due to unfavorable environmental conditions. The preferred habitat for *H. longicornis* is thought to be the oligotrophic subtropical gyres, while areas of high production and high nutrients, such as the upwelled waters of the equatorial region, are marked by low abundance and low reproductive success of *H. longicornis* (Chapter 1; E. Goetze unpubl.). Additionally, the NBC is injected with ~80,000-250,000 m<sup>3</sup> s<sup>-1</sup> of freshwater carrying ~36.1 Tg yr<sup>-1</sup> total organic carbon and ~1.2 x 10<sup>9</sup> m<sup>3</sup>/yr of suspended sediments from the Amazon River (Meade et al., 1985; Oltman, 1968; Muller-Karger et al., 1988; Richey et al., 1990), indicating that the NBC is likely poor habitat for *H. longicornis*. Thus, contemporary dispersal among subtropical gyres via either the NBC or the interior of the Atlantic Ocean basin is unlikely due to the long equatorial residence times

for copepods in a region that is unsuitable for survival and/or reproduction of multiple generations.

The equatorial region and the NBC likely also serve as biophysical dispersal barriers for other holoplanktonic species. Bimodal patterns of abundance, with high abundance in the subtropical gyres and low abundance in the equatorial region, have been reported for other copepod species (e.g. *Clausocalanus paululus*, *C. parapergens*, Schnack-Schiel et al., 2010; *Pleuromamma xiphias*, E. Goetze unpubl.), suggesting that the equatorial region may be unsuitable habitat for a number of species that inhabit the lower epipelagic and upper mesopelagic zones. For these species, as well as *H. longicornis*, the environmental factors that drive these abundance patterns are unknown, but high mortality and/or low reproduction may occur due to a variety of factors, including increased predation or exposure to metabolically unsuitable conditions, such as decreased temperature. However, the strength and importance of the equatorial dispersal barrier may vary across species, depending on the preferred habitat depth. Current velocities tend to be faster at shallower depths. In the NBC, the current shear is dramatic, and current velocities decline from  $\sim 75 - 250 \text{ cm s}^{-1}$  in surface waters to  $\sim 20 - 40 \text{ cm s}^{-1}$  at depths below the thermocline (between 150 and 200 m; Flagg et al., 1986). As a result, dispersal in near surface layers may be up to 10 times faster than dispersal at 200 m. This would mean that organisms living in the upper 20 m could migrate through the equatorial region in as little as 18 days (instead of 6 months, at 200 m depth). For organisms with a lifespan of  $\sim 1$  month, this transit across the equatorial region may be feasible and connectivity among subtropical gyre populations could be high, even if the equatorial region is poor quality habitat. Conversely, dispersal of organisms living at deeper depths would occur more slowly, making it even less likely that migrants would successfully

disperse among subtropical gyres under similar circumstances (poor quality habitat in equatorial regions).

#### *Dispersal among gyres in the Pacific Ocean*

Genetic divergence among subtropical gyre populations was observed for *H. longicornis* in the Pacific as well as the Atlantic Ocean (Chapter 1), and the equatorial region also likely serves as a dispersal barrier in this ocean basin. This pattern of genetic structure has been reported for a few other holoplanktonic species (Goetze, 2005, 2011), and it probably occurs more often than is reported because detection of these genetic patterns requires basin-scale sampling, which remains rare. However, the mechanisms driving these patterns of genetic divergence among subtropical gyre populations in the Pacific are unknown. One difference between the oceanography of the Atlantic and Pacific Oceans is that the Pacific has no meridional current that traverses the equatorial region, analogous to the Atlantic's NBC, which would provide a dispersal pathway among subtropical gyre regions (Qu and Lindstrom, 2002). Therefore, it is possible that physical oceanography alone plays a greater role in creating a dispersal barrier between subtropical gyres in the equatorial Pacific. On the other hand, the westward flowing South Equatorial Current (SEC) feeds into the Hiri Current or the North Queensland Current at ~12°S, which follows the coastline of Papua New Guinea. This feeds into the New Guinea Coastal Undercurrent, which continues to travel northwestward, transporting water from the subtropics to the equatorial region (Qu and Lindstrom, 2002). Although it is unclear if there is a pathway from the equator to the northern subtropical gyre, a circuitous route may exist for migrants to disperse among subtropical gyre habitats.

### *Isolation by oceanographic distance*

Dispersal probability was a poor predictor for genetic distance at the subtropical gyre scale (Fig. 11), and was not an improvement on Euclidean distance for understanding spatial patterns in genetic differentiation among sites in *H. longicornis*. Why was this approach uninformative for this holoplanktonic species, when modeling studies on meroplankton have found that simulated larval dispersal distance is a good predictor for genetic distance among benthic populations (White et al., 2010; Alberto et al., 2011)? First and foremost, it is possible that a pattern of IBD is unlikely to develop in pelagic species due to the dynamic spatial structure, though it has been reported in a few studies on either planktonic or pelagic organisms (Casteleyn et al., 2010; Goetze, 2011; Purcell and Edmands, 2011). A pattern of IBD is expected when nearby populations consistently exchange more migrants than distant populations, which results in adjacent populations being genetically more similar to one another than to distant populations (Wright, 1943). In the pelagic environment, the orientation of populations may change over time, in contrast to populations in stationary, benthic environments. If populations do not consistently receive differential rates of migration from nearby populations, then the genetic pattern of IBD will not develop over time. An IBD pattern is also expected under equilibrium conditions between genetic drift within populations and gene flow among them, which may not have been reached in these populations.

### *Conclusions*

Our modeling results suggest that contemporary migration likely does not occur among Atlantic subtropical gyre populations of *H. longicornis*, and that the mechanism underlying the equatorial dispersal barrier must be biophysical in nature. When particle dispersal was simulated using physical oceanographic forcing alone, the model predicted unrealistically high rates of dispersal among subtropical gyres. However, when conservative biological processes were imposed in the equatorial region to simulate poor quality habitat for this species, the model results indicated that no contemporary dispersal exists among subtropical gyre populations. Although biophysical dispersal barriers have been reported for primarily benthic species with meroplanktonic larvae (e.g. Hohenlohe, 2004; Baums et al., 2006), this is the first report of a biophysical dispersal barrier for the holoplankton. Due to the generic biological characteristics incorporated into the model, this biophysical dispersal barrier likely prevents connectivity in other mesopelagic planktonic species for whom the equatorial region is poor quality habitat. I also found that dispersal probability was a poor predictor for genetic distance, which may be explained by the dynamic pelagic habitat of this species.

## References Cited

- Alberto, F., P. T. Raimondi, D. C. Reed, J. R. Watson, D. A. Siegel, S. Mitarai, N. Coelho, and E. A. Serrao. 2011. Isolation by oceanographic distance explains genetic structure for *Macrocystis pyrifera* in the Santa Barbara Channel. *Mol. Ecol.* **20**: 2543-2554.
- Ambler, J. W., and C. Miller. 1987. Vertical habitat-partitioning by copepodites and adults of subtropical oceanic copepods. *Mar. Biol.* **94**: 561–577.
- Batchelder, H. P., C. A. Edwards, and T. M. Powell. 2002. Individual-based models of copepod populations in coastal upwelling regions: implications of physiologically and environmentally influenced diel vertical migration on demographic success and nearshore retention. *Progress in Oceanography* **53**: 307-333.
- Baums, I. B., C. B. Paris, and L. M. Chérubin. 2006. A bio-oceanographic filter to larval dispersal in a reef-building coral. *Limnol. Oceanogr.* **51**: 1969–1981.
- Bi, H., K. A. Rose, and M. C. Benfield. 2011. Estimating copepod stage-specific mortality rates in open ocean waters: a case study from the northern Gulf of Mexico, USA. *Mar. Ecol. Prog. Ser.* **427**: 145-159.
- Breteler, W.C.M.K. 1980. Continuous breeding of marine pelagic copepods in the presence of heterotrophic dinoflagellates. *Mar. Ecol. Prog. Ser.* **2**: 229-233.
- Bryant, A. D., D. Hainbucher, and M. Heath. 1998. Basin-scale advection and population persistence of *Calanus finmarchicus*. *Fish. Oceanogr.* **7**: 3/4, 235-244.

- Carton, J. A., G. A. Chepurin, X. Cao, and B. Giese. 2000a. A Simple Ocean Data Assimilation retrospective analysis of the global ocean 1950-1995. Part I: Methodology. *J. Phys. Oceanogr.* **30**: 294-309.
- Carton, J. A., G. Chepurin, and X. Cao. 2000b. A Simple Ocean Data Assimilation analysis of the global upper ocean 1950-1995 Part 2: results. *J. Phys. Oceanogr.* **30**: 311-326.
- Casteleyn, G., F. Leliaert, T. Backeljau, A.-E. Debeer, Y. Kotaki, L. Rhodes, N. Lundholm, K. Sabbe, and W. Vyverman. 2010. Limits to gene flow in a cosmopolitan marine planktonic diatom. *Proc. Nat. Acad. Sci.* **107**: 12952-12957.
- Coleman, M. A., J. Chambers, N. A. Knott, H. A. Malcolm, D. Harasti, A. Jordan, and B. P. Kelaher. 2011. Connectivity within and among a network of temperate marine reserves. *PLOS One* **6**: e20168. doi:10.1371/journal.pone.0020168
- Cowen, R. K., K. M. M. Lwiza, S. Sponaugle, C. B. Paris, and D. B. Olson. 2000. Connectivity of marine populations: Open or closed? *Science* **287**: 857-859.
- Cowen, R. K., and S. Sponaugle. 2009. Larval dispersal and marine population connectivity. *Annu. Rev. Mar. Sci.* **1**: 443-466.
- Dawson, M. N., A.S. Gupta, and M. H. England. 2005. Coupled biophysical global ocean model and molecular genetic analyses identify multiple introductions of cryptogenic species. *Proc. Nat. Acad. Sci.* **102**: 11968-11973.
- Excoffier, L., and H. E. L. Lischer. 2010. Arlequin suite version 3.5: A new series of programs to perform population genetics analyses under Linux and Windows. *Mol. Ecol. Resour.* **10**: 564-567.

- Flagg, C. N., R. L. Gordon, and S. McDowell. 1986. Hydrographic and current observations on the continental slope and shelf of the western equatorial Atlantic. *J. Phys. Oceanogr.* **16**: 1412-1429.
- Ferguson, A., J. B. Taggart, P. A. Prodohl, O. McMeel, C. Thompson, C. Stone, P. McGinnity, and R. A. Hynes. 1995. The application of molecular markers to the study and conservation of fish populations, with special reference to *Salmo*. *J. Fish Biol.* **47**: 103-126.
- Gilg, M. R., and T. J. Hilbish. 2003. The geography of marine larval dispersal: Coupling genetics with fine-scale physical oceanography. *Ecol.* **84**: 2989-2998.
- Goetze, E. 2005. Global population genetic structure and biogeography of the oceanic copepods *Eucalanus hyalinus* and *E. spinifer*. *Evolution* **59**: 2378–2398.
- Goetze, E. 2011. Population differentiation in the open sea: insights from the pelagic copepod *Pleuromamma xiphias*. *Integr. Comp. Biol.* **51**: 580–597.
- Hirst, A. G., and A. J. Bunker. 2003. Growth of marine planktonic copepods: Global rates and patterns in relation to chlorophyll *a*, temperature, and body weight. *Limnol. Oceanogr.* **48**: 1988-2010.
- Hirst, A. G., and T. Kiorboe. 2002. Mortality of marine planktonic copepods: global rates and patterns. *Mar. Ecol. Prog. Ser.* **230**: 195-209.
- Hohenlohe, P. A. 2004. Limits to gene flow in marine animals with planktonic larvae: models of *Littorina* species around Point Conception, California. *Biol. J. Linn. Soc.* **82**: 169-187.

- Hopkins, T. L. 1985. Food web of an Antarctic midwater ecosystem. *Mar. Biol.* **89**: 197-212.
- Johns, W. E., T. N. Lee, F. A. Schott, R. J. Zantopp, and R. H. Evans. 1990. The North Brazil Current retroflection: seasonal structure and eddy variability. *J. Geophys. Res.* **95**: 22,103-22,120.
- Joyeux, J.-C., S. R. Floeter, C. E. L. Ferreira, and J. L. Gasparini. 2001. Biogeography of tropical reef fishes: the South Atlantic puzzle. *J. Biogeogr.* **28**: 831-841.
- Keeney, D. B., and E. J. Heist. 2006. Worldwide phylogeography of the blacktip shark (*Carcharhinus limbatus*) inferred from mitochondrial DNA reveals isolation of western Atlantic populations coupled with recent Pacific dispersal. *Mol. Ecol.* **15**: 3669-3679.
- Kimmerer, W. J., and A. D. McKinnon. 1987. Growth, mortality, and secondary production of the copepod *Acartia tranteri* in Westernport Bay, Australia. *Limnol. Oceanogr.* **32**: 14-28.
- Knowlton, N., and L. A. Weigt. 1998. New dates and new rates for divergence across the Isthmus of Panama. *Proc. Roy. Soc. B* **265**: 2257-2263.
- Kool, J. T., C. B. Paris, S. Andrefouet, and R. K. Cowen. 2010. Complex migration and the development of genetic structure in subdivided populations: An example from Caribbean coral reef ecosystems. *Ecography* **33**: 597-606.
- Kool, J. T., C. B. Paris, P. H. Barber, and R. K. Cowen. 2011. Connectivity and the development of population genetic structure in Indo-West Pacific coral reef communities. *Global Ecol. Biogeogr.* **20**: 695-706.

- Lessios, H. A., and D. R. Robertson. 2006. Crossing the impassable: genetic connections in 20 reef fishes across the eastern Pacific barrier. *Proc. Roy. Soc. B* **273**: 2201-2208.
- Longhurst, A. R. 2007. *Ecological geography of the sea*. Academic Press.
- Marko, P. B., and M. W. Hart. 2011. The complex analytical landscape of gene flow inference. *Trends Ecol. Evol.* **26**: 448-456.
- McGowan, J. A., and P. W. Walker. 1979. Structure in the copepod community of the North Pacific central gyre. *Ecol. Monogr.* **49**: 195-226.
- Meade, R. H., T. Dunne, J. E. Richey, U. D. M. Santos, and E. Salati. 1985. Storage and remobilization of suspended sediment in the lower Amazon River of Brazil. *Science* **228**: 488-490.
- Metcalf, W. G., and M. C. Stalcup. 1967. Origin of the Atlantic Equatorial Undercurrent. *J. Geophys. Res.* **72**: 4959-4975.
- Mills, L. S., and F. W. Allendorf. 1996. The one-migrant-per-generation rule in conservation and management. *Conserv. Biol.* **10**: 1509-1518.
- Mora, C., and P. F. Sale. 2002. Are populations of coral reef fish open or closed? *Trends Ecol. Evol.* **17**: 422-428.
- Muller-Karger, F. E., C. R. McClain, and P. L. Richardson. 1988. The dispersal of the Amazon's waters. *Nature* **333**: 56-69.
- Murphy, E. J., J. L. Watkins, K. Reid, P. N. Trathan, I. Everson, J. P. Croxall, J. Priddle, M. A. Brandon, A. S. Brierley, and E. Hofmann. 1998. Interannual variability of the

- South Georgia marine ecosystem: biological and physical sources of variation in the abundance of krill. *Fish. Oceanogr.* **7**: ¾, 381-390.
- North, E. W., Z. Schlag, R. R. Hood, M. Li, L. Zhong, T. Gross, and V. S. Kennedy. 2008. Vertical swimming behavior influences the dispersal of simulated oyster larvae in a coupled particle-tracking and hydrodynamic model of Chesapeake Bay. *Mar. Ecol. Prog. Ser.* **359**: 99-115.
- Ohman, M. D., K. Eiane, E. G. Durbin, J. A. Runge, and H.-J. Hirche. 2004. A comparative study of *Calanus finmarchicus* mortality patterns at five localities in the North Atlantic. *ICES J. Mar. Sci.* **61**: 687-697.
- Oltman, R. E. 1968. Reconnaissance investigations of the discharge and water quality of the Amazon River. U. S. Geological Survey, Circular 552.
- Palsboll, P. J., M. Berube, and F. W. Allendorf. 2007. Identification of management units using population genetic data. *Trends in Ecol. Evol.* **22**: 11-16.
- Palumbi, S. R. 2003. Population genetics, demographic connectivity, and the design of marine reserves. *Ecol. Appl.* **13**: S146-S158.
- Paris, C. B., L. M. Chérubin, and R. K. Cowen. 2007. Surfing, spinning, or diving from reef to reef: effects on population connectivity. *Mar. Ecol. Prog. Ser.* **347**: 285-300.
- Peijnenburg, KTCA., E. K. van Haastrecht, and C. Fauvelot. 2005. Present-day genetic composition suggests contrasting demographic histories of two dominant chaetognaths of the North-East Atlantic, *Sagitta elegans* and *S. setosa*. *Mar. Biol.* **147**: 1279–1289.

- Peterson, W. T. 1985. Abundance, age structure and in situ egg production rates of the copepod *Temora longicornis* in Long Island Sound, New York. *Bull. Mar. Sci.* **37**: 726-738.
- Pogson, G. H., C. T. Taggart, K. A. Mesa, and R. G. Boutilier. 2001. Isolation by distance in the Atlantic cod, *Gadus morhua*, at large and small geographic scales. *Evol.* **55**: 131-146.
- Pringle, J. M., and J. P. Wares. 2007. Going against the flow: Maintenance of alongshore variation in allele frequency in a coastal ocean. *Mar. Ecol. Prog. Ser.* **335**: 69-84.
- Purcell, C. M., and S. Edmands. 2011. Resolving the genetic structure of the striped marlin, *Kajikia audax*, in the Pacific Ocean through spatial and temporal sampling of adult and immature fish. *Can. J. Fish. Aquat. Sci.* **68**: 1861-1875.
- Qu, T., and E. J. Lindstrom. 2002. A climatological interpretation of the circulation in the Western South Pacific. *J. Phys. Oceanogr.* **32**: 2492-2508.
- Razouls, C., F. de Bovee, J. Kouwenberg, and N. Desreumaux. 2005-2012. Diversity and geographic distribution of marine planktonic copepods. Available at <http://copepodes.obs-banyuls.fr/en> [Accessed 17 May 2013]
- Reid, J. L., Jr. 1964. A transequatorial Atlantic oceanographic section in July 1963 compared with other Atlantic and Pacific sections. *J. Geophys. Res.* **69**: 5205-5215.
- Richardson, P. L., G. E. Huffor, R. Limeburner, and W. S. Brown. 1994. North Brazil Current retroflexion eddies. *J. Geophys. Res.* **99**: 5081-5093.

- Richardson, P. L., and G. Reverdin. 1987. Seasonal cycle of velocity in the Atlantic North Equatorial Countercurrent as measured by surface drifters, current meters, and ship drifts. *J. of Geophys. Res.* **92**: 3691-3708.
- Richey, J. E., J. B. Adams, and R. L. Victoria. 1990. Synoptic-scale hydrological and biogeochemical cycles in the Amazon River basin: A modeling and remote sensing perspective. In R. J. Hobbs and H. A. Mooney (Eds.), *Remote sensing of biosphere functioning* (pp. 249-268). New York: Springer-Verlag.
- Robins, P. E., S. P. Neill, L. Gimenez, S. R. Jenkins, and S. K. Malham. 2013. Physical and biological controls on larval dispersal and connectivity in a highly energetic shelf sea. *Limnol. Oceanogr.* **58**: 505-524.
- Rocha, L. A. 2003. Patterns of distribution and processes of speciation in Brazilian reef fishes. *J. Biogeogr.* **30**: 1161–1171.
- Rocha, L. A., M. T. Craig, and B. W. Bowen. 2007. Phylogeography and the conservation of coral reef fishes. *Coral Reefs* **26**: 501–512.
- Rousset, F. 1997. Genetic differentiation and estimation of gene flow from *F*-statistics under isolation by distance. *Genetics* **145**: 1219–1228.
- Saraladevi, K., R. Stephen, and T. S. S. Rao. 1979. Distribution of *Haloptilus* (Copepoda, Calanoida) in the Indian Ocean. *Indian J. Mar. Sci.* **8**: 159–165.
- Schnack-Schiel, S. B., E. Mizdalski, and A. Cornils. 2010. Copepod abundance and species composition in the Eastern subtropical/tropical Atlantic. *Deep-Sea Res. II* **57**: 2064–2075.

- Schott, F. A., J. Fischer, and L. Stramma. 1998. Transports and pathways of the upper-layer circulation in the Western tropical Atlantic. *J. Phys. Oceanogr.* **28**: 1904–1928.
- Schott, F. A., P. Brandt, M. Hamann, J. Fischer, and L. Stramma. 2002. On the boundary flow off Brazil at 5-10°S and its connection to the interior tropical Atlantic. *Geophys. Res. Lett.* **29**: 21-1 – 21-4.
- Schubart, C. D., R. Diesel, and S. B. Hedges. 1998. Rapid evolution to terrestrial life in Jamaican crabs. *Nature* **393**: 363-365.
- Siegel DA, Kinlan BP, Gaylord B, Gaines SD. 2003. Lagrangian descriptions of marine larval dispersion. *Mar. Ecol. Prog. Ser.* **260**: 83-96.
- Slatkin, M. 1985. Gene flow in natural populations. *Annu. Rev. Ecol. Syst.* **16**: 393-430.
- Slatkin, M. 1987. Gene flow and geographic structure of natural populations. *Science* **236**: 787-792.
- Speirs DC, Gurney WSC, Heath MR, Wood SN. 2005. Modeling the basin-scale demography of *Calanus finmarchicus* in the north-east Atlantic. *Fish. Oceanogr.* **15**: 333-358
- Speirs DC, Gurney WSC, Heath MR, Horbelt W, Wood SN, de Cuevas BA. 2006. Ocean-scale modeling of the distribution, abundance, and seasonal dynamics of the copepod *Calanus finmarchicus*. *Mar. Ecol. Prog. Ser.* **313**: 173-192.
- Spieth, P. T. 1974. Gene flow and genetic differentiation. *Genetics* **78**: 961-965.
- Tajima, F. 1996. The amount of DNA polymorphism maintained in a finite population when the neutral mutation rate varies among sites. *Genetics* **143**:1457-1465.

- Treml EA, Halpin PN, Urban DL, Pratson LF. 2008. Modeling population connectivity by ocean currents, a graph-theoretic approach for marine conservation. *Landscape Ecol.* **23**: 19-36.
- Vucetich, J. A., and T. A. Waite. 2000. Is one migrant per generation sufficient for the genetic management of fluctuating populations? *Anim. Conserv.* **3**: 261-266.
- Warner, R. R., and R. K. Cowen. 2002. Local retention of production in marine populations: evidence, mechanisms, and consequences. *Bull. Mar. Sci.* **70**: 245-249.
- White C, Selkoe KA, Watson J, Siegel DA, Zacherl DC, Toonen RJ. 2010. Ocean currents help explain population genetic structure. *Proc. Roy. Soc. B* **277**:1685-1694.
- Whitlock, M. C., and D. E. McCauley. 1999. Indirect measures of gene flow and migration:  $F_{ST} \neq 1/(4Nm+1)$ . *Heredity* **82**: 117-125.
- Wirth, T., and L. Bernatchez. 2001. Genetic evidence against panmixia in the European eel. *Nature* **409**: 1037-1040.
- Wright, S. 1931. Evolution in Mendelian populations. *Genetics* **16**: 97-159.

## Tables

Table 1. Station locations for genetic data and particle releases in Experiment 2 (IBOD). Site – collection site number (see Fig. 4), Sample – cruise name and station number,  $n$  – number of individuals sequenced, including only mtDNA haplotype group 1. Station locations shown in Figure 4.

<b>Site</b>	<b>Sample</b>	<b>Latitude</b>	<b>Longitude</b>	<b>Date</b>	<b><math>n</math></b>
1	AMT20-28	-29.943	-31.690	11/16/2010	14
2	AMT20-26	-23.838	-26.567	11/14/2010	24
3	AMT20-24	-15.331	-21.841	11/11/2010	21
4	MP3-14-01-00	12.038	-55.262	7/8/2001	24
5	AMT20-16	13.455	-38.950	10/30/2010	19
6	AMT20-15	16.190	-35.806	10/29/2010	21
7	AMT20-13	21.212	-39.293	10/27/2010	26
8	AMT20-11	25.985	-38.783	10/25/2010	27
9	MP3-12-06-00	29.570	-45.026	7/2/2001	10
10	MP3-08-03-00	29.427	-35.564	6/30/2001	25
11	AMT20-9	30.288	-34.181	10/23/2010	28
12	AMT20-7	34.203	-29.722	10/21/2010	11
13	MP3-02-06-00	29.096	-23.361	6/27/2001	25

Table 2. Pairwise  $F_{ST}$  values between all collection sites in the Atlantic Ocean. Sample numbers correspond to those in Table 1. Significance levels for  $F_{ST}$  values are indicated by underline ( $p \leq 0.000067$ , significant after Bonferroni correction) and **bold** ( $p \leq 0.05$ ). Within-gyre comparisons are italicized.

	1	2	3	4	5	6	7	8	9	10	11	12	13
1	*												
2	<i>0.048</i>	*											
3	<i>0.026</i>	<i>0.005</i>	*										
4	<b>0.159</b>	<u>0.274</u>	<u>0.204</u>	*									
5	<b>0.201</b>	<u>0.327</u>	<u>0.248</u>	<i>-0.007</i>	*								
6	<b>0.209</b>	<u>0.326</u>	<u>0.253</u>	<i>-0.011</i>	<i>-0.037</i>	*							
7	<u>0.265</u>	<u>0.379</u>	<u>0.304</u>	<i>0.007</i>	<i>-0.032</i>	<i>-0.023</i>	*						
8	<b>0.198</b>	<u>0.317</u>	<u>0.243</u>	<i>-0.022</i>	<i>-0.032</i>	<i>-0.030</i>	<i>-0.021</i>	*					
9	<b>0.179</b>	<b>0.308</b>	<b>0.229</b>	<i>-0.058</i>	<i>-0.052</i>	<i>-0.052</i>	<i>-0.051</i>	<i>-0.062</i>	*				
10	<b>0.181</b>	<u>0.297</u>	<u>0.226</u>	<i>-0.025</i>	<i>-0.027</i>	<i>-0.027</i>	<i>-0.015</i>	<i>-0.030</i>	<i>-0.062</i>	*			
11	<u>0.296</u>	<u>0.403</u>	<u>0.331</u>	<i>0.012</i>	<i>-0.013</i>	<i>-0.007</i>	<i>-0.027</i>	<i>-0.012</i>	<i>-0.041</i>	<i>-0.003</i>	*		
12	<b>0.259</b>	<u>0.378</u>	<u>0.301</u>	<i>0.004</i>	<i>-0.040</i>	<i>-0.047</i>	<i>-0.028</i>	<i>-0.031</i>	<i>-0.040</i>	<i>-0.018</i>	<i>-0.018</i>	*	
13	<u>0.406</u>	<u>0.493</u>	<u>0.427</u>	<b>0.089</b>	<i>0.019</i>	<i>0.022</i>	<i>0.002</i>	<i>0.037</i>	<i>0.040</i>	<i>0.052</i>	<i>0.001</i>	<i>-0.027</i>	*

## Figures

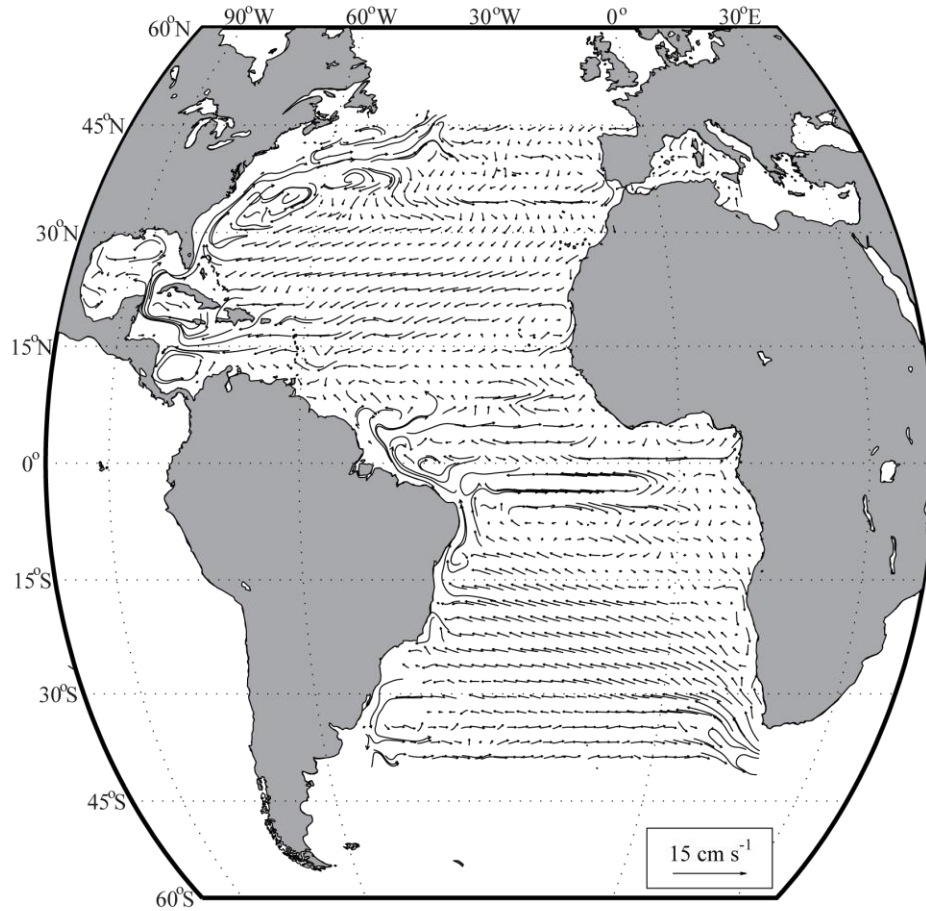


Figure 1. Ocean velocities at the 197 m depth layer averaged over the entire temporal span of the ocean circulation model, from years 1871 to 2008. The length of the vector is proportional to the magnitude of the velocity, according to the scale vector.

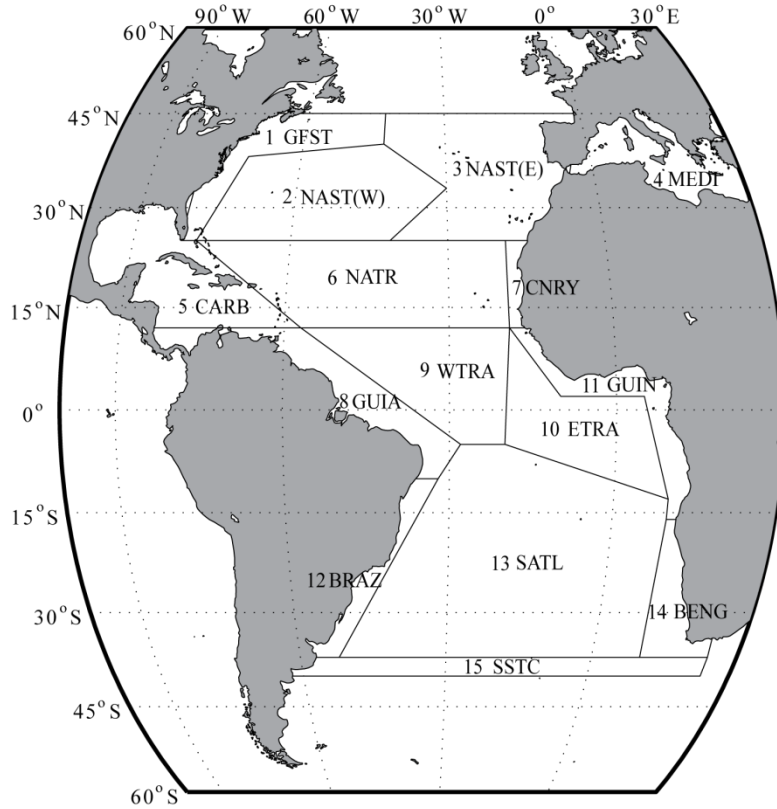


Figure 2. The Atlantic Ocean divided into 15 regions as defined by Longhurst (2007).

Model bounds were set at 45 °N and 40 °S, which represent the distributional limits for this species. We consider regions 2 and 6 together as the northern subtropical gyre, and region 13 represents the southern subtropical gyre; the equatorial region consists of regions 8-11. 1) GFST = Gulf Stream; 2) NAST(W) = North Atlantic Subtropical Gyre (West), 3) NAST(E) = North Atlantic Subtropical Gyre (East), 4) MEDI = Mediterranean Sea, 5) CARB = Caribbean, 6) NATR = North Atlantic Tropical Gyre, 7) CNRY = Canary Current, 8) GUIA = Guianas, 9) WTRA = Western Tropical Atlantic, 10) ETRA = Eastern Tropical Atlantic, 11) GUIN = Guinea Current, 12) BRAZ = Brazil Current, 13) SATL = South Atlantic Gyre, 14) BENG = Benguela Current, 15) SSTC = South Subtropical Convergence (Longhurst, 2007).

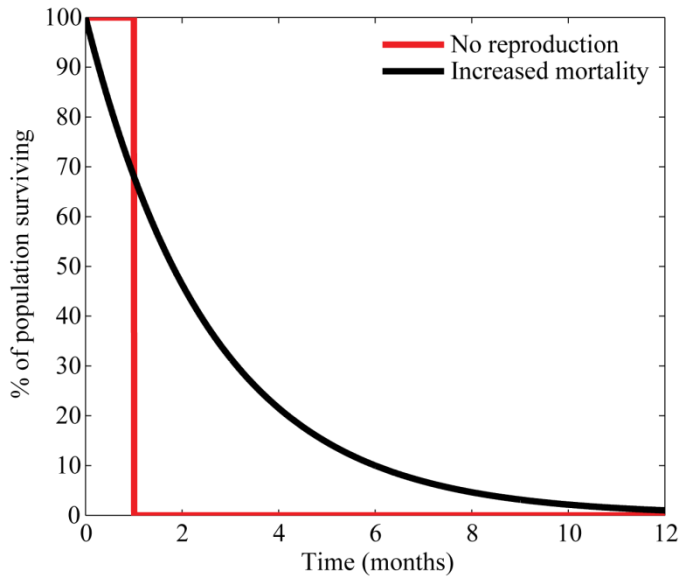


Figure 3. To simulate lower quality habitat in the equatorial region, biological processes were simulated in two ways: (1) through increased mortality in equatorial waters, using an exponential decay function to decrease the population to 1% of its initial size after one year (black curve), and (2) through an absence of reproduction in equatorial waters, by terminating all particles that were in equatorial regions for more than 30 consecutive days (~ 1 generation; red curve).

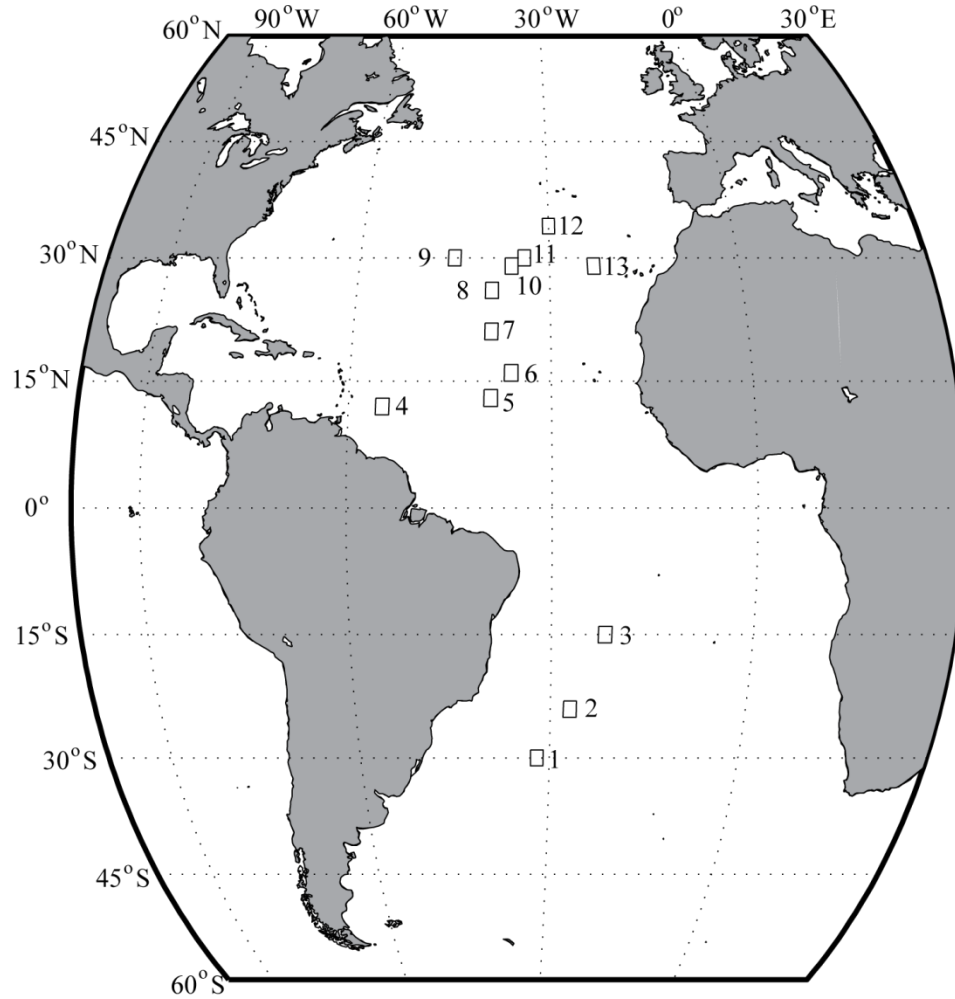


Figure 4. Station locations in the Atlantic Ocean that were used for particle release experiments in isolation by oceanographic distance (IBOD) simulations. These locations correspond to plankton sampling stations from which we have genetic data for *H. longicornis* (see Table 1).

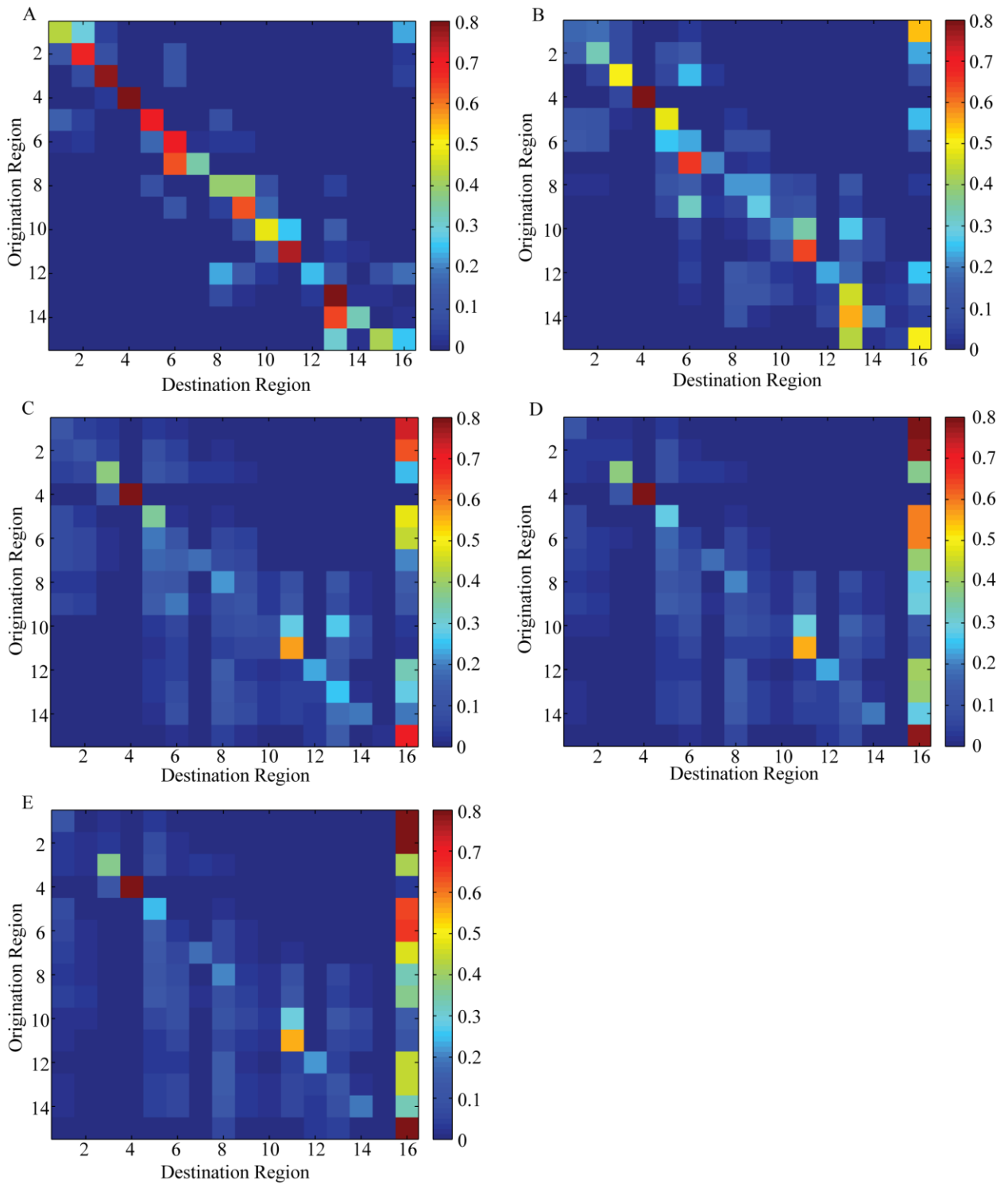


Figure 5. Connectivity matrices showing the dispersal probability of particles to different regions in the Atlantic Ocean after (A) 1 year, (B) 5 years, (C) 15 years, (D) 25 years, and (E) 30 years. Regions are defined as in Figure 2, with the exception that “Region 16”

represents the particles that are no longer viable. Subtropical gyres correspond to regions 2 and 6 (northern) and region 13 (southern). Squares along the diagonal represent local retention rates within a region.

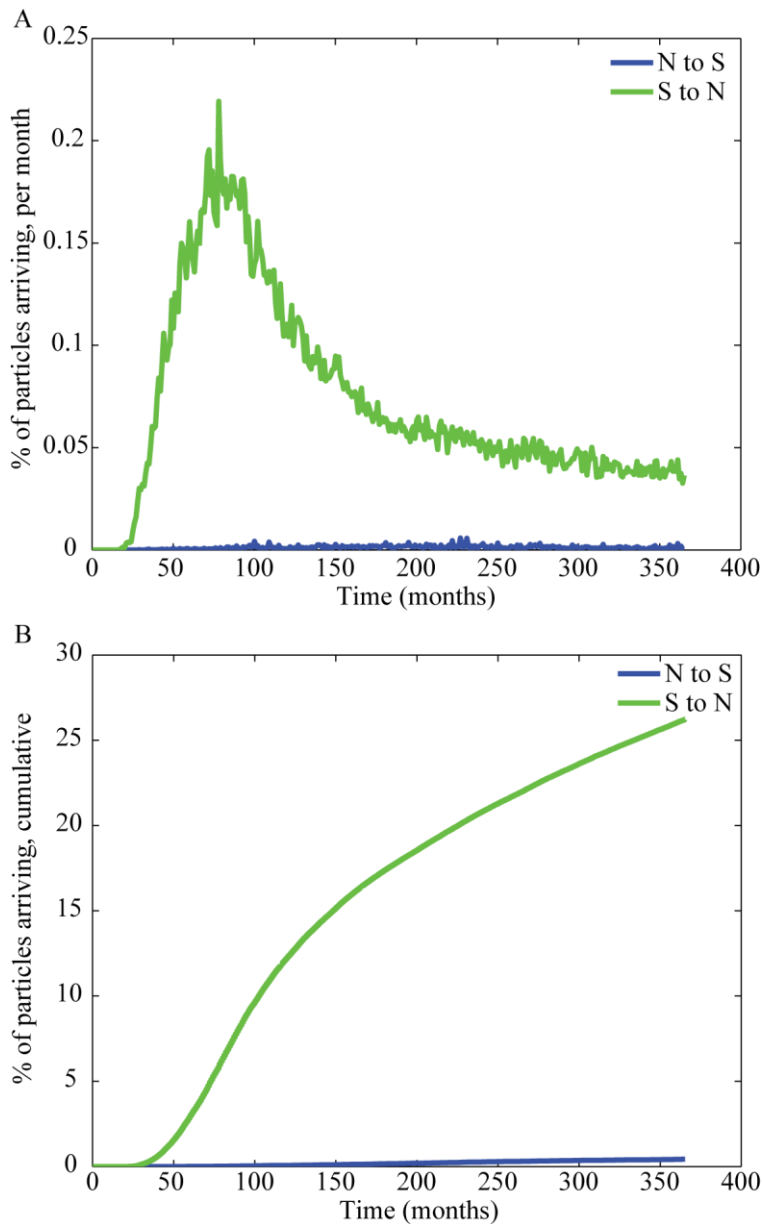


Figure 6. Migration among Atlantic subtropical gyres, over a 30-year simulation. Percent of unique particles that successfully dispersed to the opposite subtropical gyre (A) per month and (B) cumulative over time. In both plots, particles moving from the southern to the northern subtropical gyre are shown in green; blue indicates particles traveling from the northern to the southern subtropical gyre.

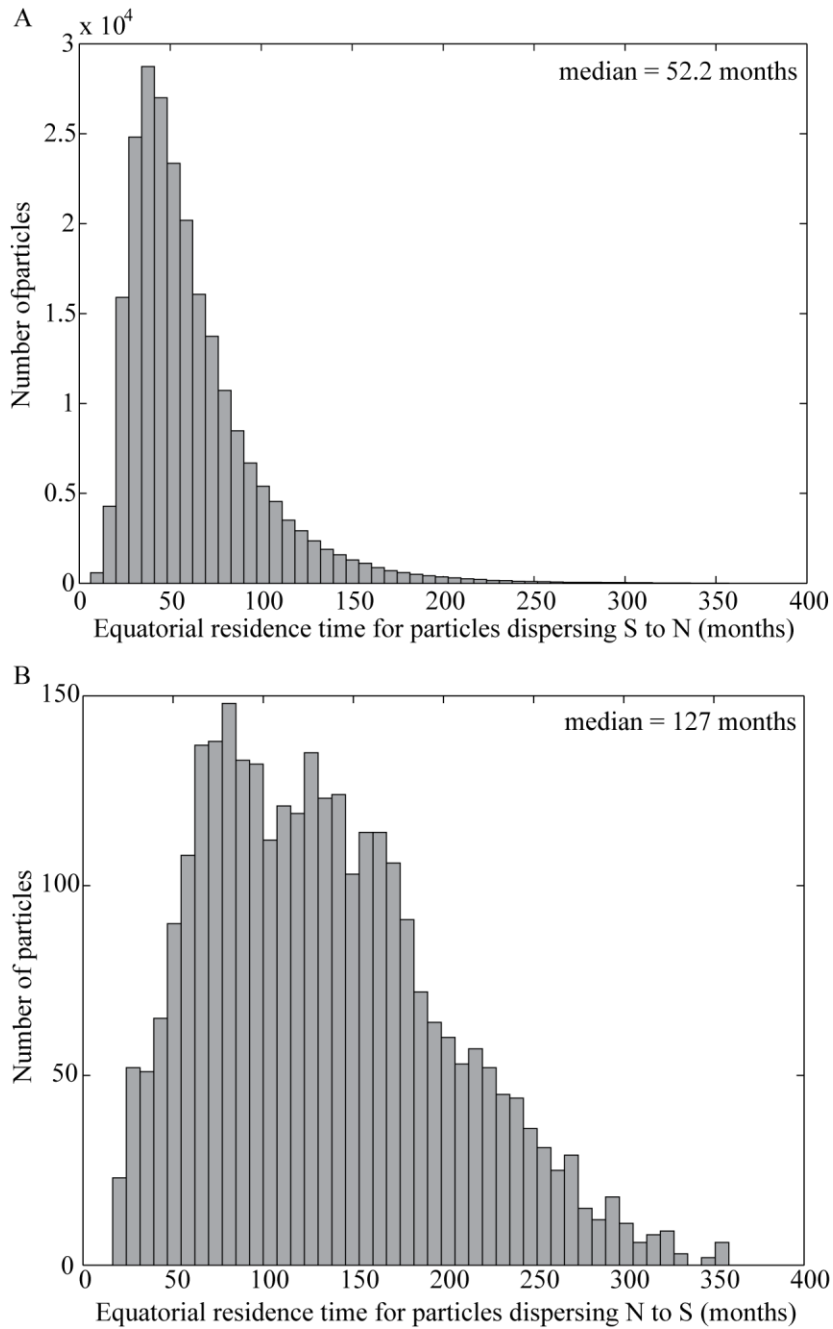


Figure 7. Residence times in the Atlantic equatorial region (in months) for particles dispersing from (A) the southern to the northern subtropical gyre, and (B) the northern to the southern subtropical gyre. Note the difference in scale on the y-axis between plots in A and B.

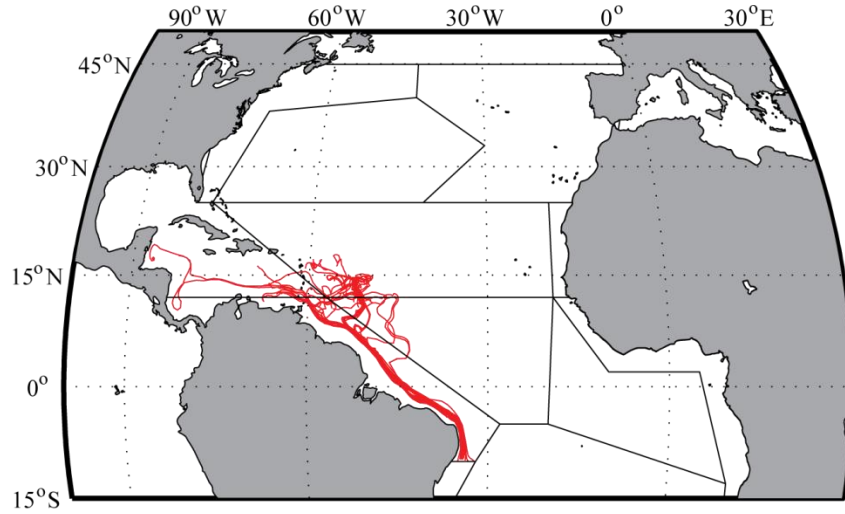


Figure 8. Dispersal trajectories for the fastest particles that successfully dispersed from the southern to the northern subtropical gyre (across equatorial waters in region 8). Only these 26 particles had equatorial residence times less than 8 months. Trajectories are shown for an additional 8 months after the particles exited the equatorial region.

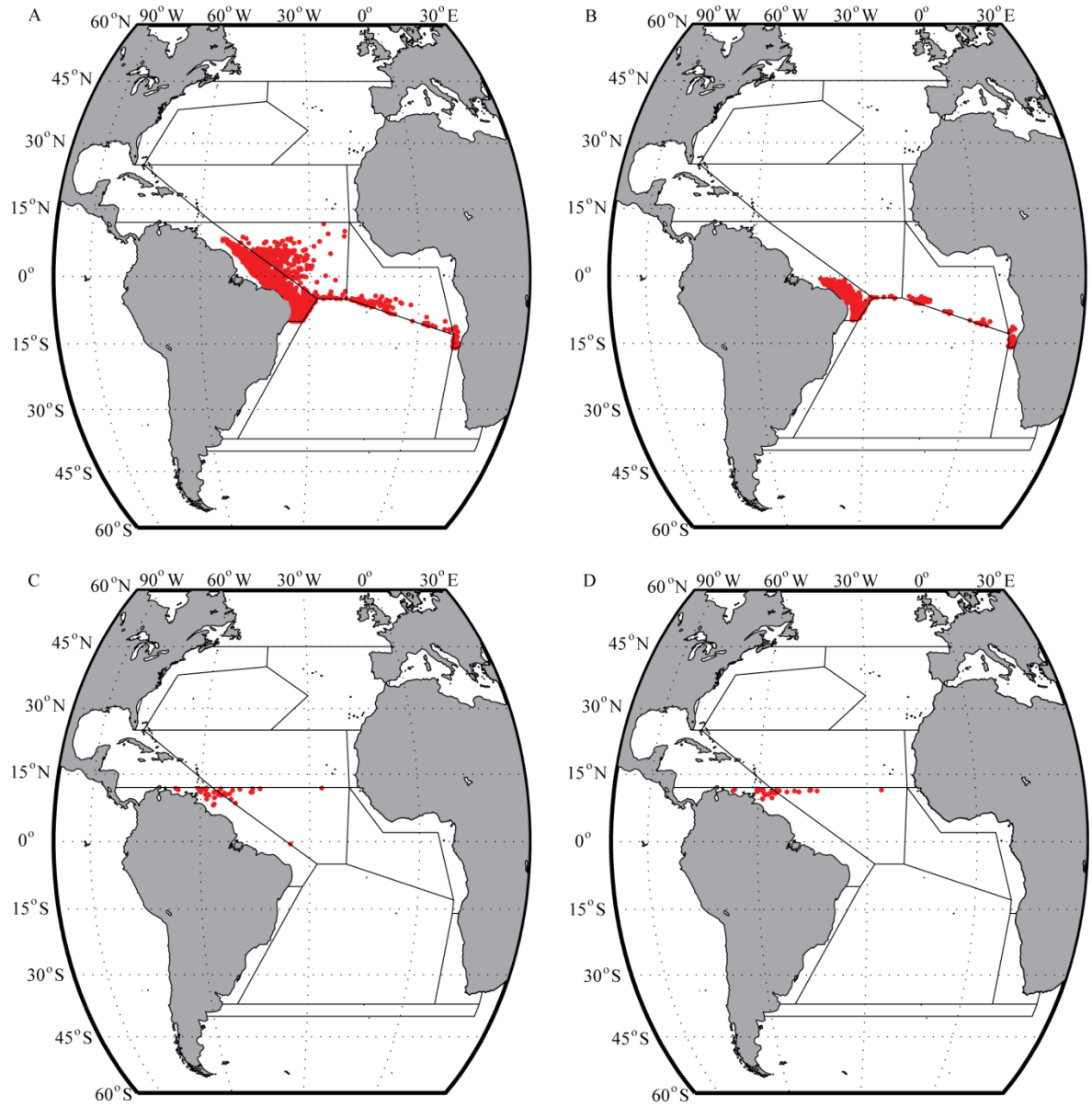


Figure 9. Death locations for particles dispersing across the equatorial region from the southern to the northern subtropical gyre under (A) increased mortality and (B) decreased reproduction, and from the northern to the southern subtropical gyre under (C) increased mortality and (D) decreased reproduction.

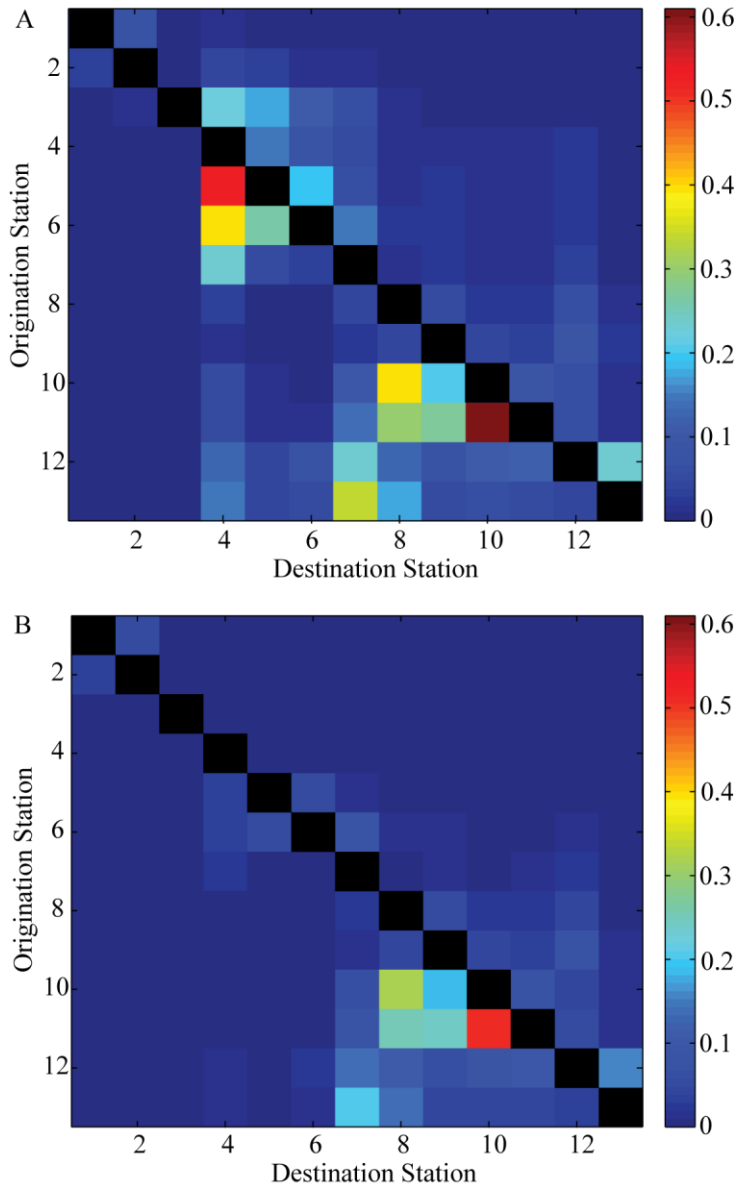


Figure 10. Average dispersal probabilities among Atlantic Stations when (A) physical forcing alone was used to simulate dispersal of particles, and (B) when increased mortality was imposed in the equatorial region. The same results (as shown in B) were observed when decreased reproduction was imposed in the equatorial region (data not shown). Note: retention within stations was not calculated (i.e. black squares along the diagonal). Station numbers are the same as in Table 1.

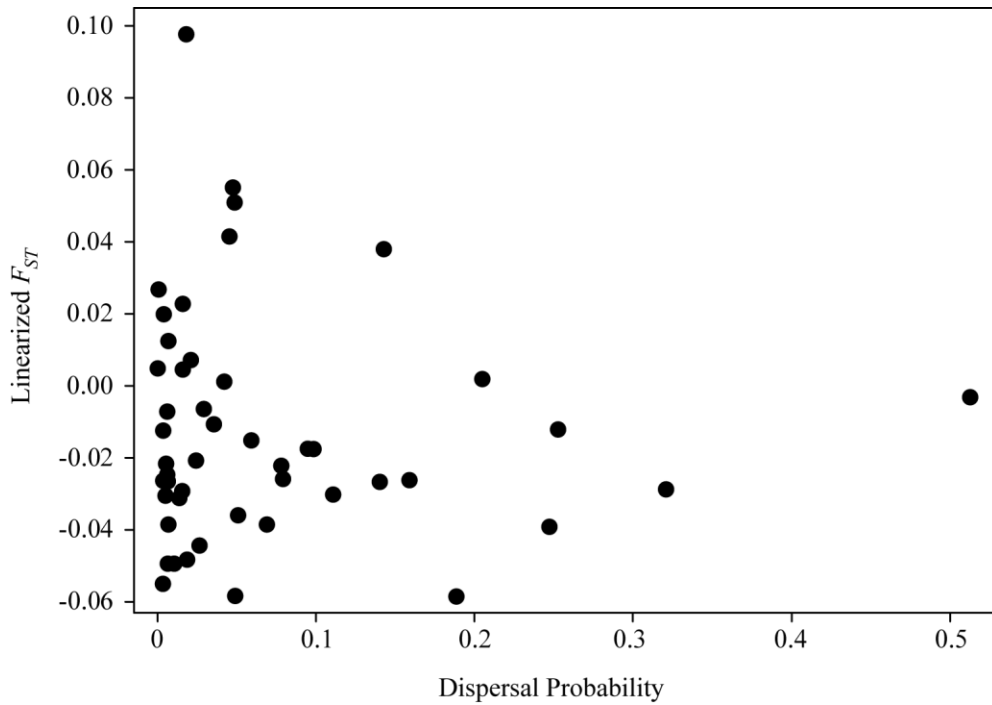


Figure 11. Linearized  $F_{ST}$  versus maximum dispersal probability for within gyre station comparisons (for mtDNA Group 1 only) when mortality was simulated in the equatorial region. There was no significant relationship between these parameters (linear regression,  $p > 0.05$ ). Note that dispersal probability was zero for all among gyre comparisons, and the same results were obtained when decreased reproduction was simulated in the equatorial region (results not shown).

## **Future work**

Few pelagic dispersal barriers have been identified for members of the holoplankton community, and the mechanisms driving these barriers are not well understood. Although I have identified an equatorial dispersal barrier for *H. longicornis* (Chapter 2), future work should be conducted to understand how formidable this dispersal barrier is for other holoplankton species and to identify other potential dispersal barriers. This could be done by sampling a wide range of holoplankton species on a global scale and conducting genetic studies in order to detect genetic breaks between populations. Ocean circulation models coupled with individual based models (IBMs) could also be used to make predictions about locations of potential physical or biophysical dispersal barriers. IBMs would allow the incorporation of known biological characteristics of a marine species into the model, such as habitat depth, vertical migration behavior, feeding requirements, and life history characteristics (e.g. Bryant et al., 1998; Baums et al., 2006; North et al., 2008). Changes in vertical position have been shown to affect dispersal in planktonic species (e.g. Bryant et al., 1998; Batchelder et al., 2002; North et al., 2008; Robins et al., 2013), but it is currently unknown how the other factors may affect genetic connectivity in holoplankton. Genetic haplotypes could also be incorporated into the IBM (e.g. Pringle and Wares, 2007), in order to understand how genetic structure changes over time within an ocean basin, because little is known about the stability of genetic patterns for pelagic holoplankton. These model predictions could be compared to genetic data collected at the same sampling sites in different years. Congruence (or discordance) in spatial genetic patterns could be used to infer the factors determining connectivity in marine species, and to help identify additional

processes that may need to be incorporated in the model (e.g., selection for/against migrants; Galindo et al., 2010).

For *H. longicornis* specifically, it would be interesting to further investigate the biophysical interactions in the equatorial region that cause increased mortality or decreased reproduction for this species. This would require a broader knowledge of the physiological requirements of *H. longicornis*, which could be gained by conducting experiments with live animals collected from the preferred subtropical gyre regions of the Atlantic. Also, we could investigate the mechanisms driving other genetic breaks (e.g. in the equatorial Pacific, between the Pacific and the Indian Ocean populations) or regions of high connectivity (e.g. between the Indian and the South Atlantic populations) using a different domain of the global SODA model.

## References

- Batchelder, H. P., C. A. Edwards, and T. M. Powell. 2002. Individual-based models of copepod populations in coastal upwelling regions: implications of physiologically and environmentally influenced diel vertical migration on demographic success and nearshore retention. *Progress in Oceanography* **53**: 307-333.
- Baums, I. B., C. B. Paris, and L. M. Chérubin. 2006. A bio-oceanographic filter to larval dispersal in a reef-building coral. *Limnol. Oceanogr.* **51**: 1969–1981.
- Bryant, A. D., D. Hainbucher, and M. Heath. 1998. Basin-scale advection and population persistence of *Calanus finmarchicus*. *Fish. Oceanogr.* **7**: 3/4, 235-244.
- Galindo, H. M., A. S. Pfeiffer-Herbert, M. A. McManus, Y. Chao, F. Chai, and S. R. Palumbi. 2010. Seascape genetics along a steep cline: using genetic patterns to test predictions of marine larval dispersal. *Mol. Ecol.* **19**: 3692-3707.
- North, E. W., Z. Schlag, R. R. Hood, M. Li, L. Zhong, T. Gross, and V. S. Kennedy. 2008. Vertical swimming behavior influences the dispersal of simulated oyster larvae in a coupled particle-tracking and hydrodynamic model of Chesapeake Bay. *Mar. Ecol. Prog. Ser.* **359**: 99-115.
- Pringle, J. M., A. M. H. Blakeslee, J. E. Byers, and J. Roman. 2011. Asymmetric dispersal allows an upstream region to control population structure throughout a species' range. *Proc. Natl. Acad. Sci.*

Robins, P. E., S. P. Neill, L. Gimenez, S. R. Jenkins, and S. K. Malham. 2013. Physical and biological controls on larval dispersal and connectivity in a highly energetic shelf sea. *Limnol. Oceanogr.* **58**: 505-524.